

Solution of transient viscoelastic flow problems approximated by a term-by-term VMS stabilized finite element formulation using time-dependent subgrid-scales

Laura Moreno¹, Ramon Codina^{1,2} and Joan Baiges¹

¹*Universitat Politècnica de Catalunya, Jordi Girona 1-3, Edifici C1, 08034, Barcelona, Spain*

²*Centre Internacional de Mètodes Numèrics en Enginyeria, Gran Capità S/N, 08034 Barcelona, Spain*

Abstract

Some finite element stabilized formulations for transient viscoelastic flow problems are presented in this paper. These are based on the Variational Multiscale (VMS) method, following the approach introduced in Castillo and Codina, *Comput. Meth. Appl. Mech. Eng.*, vol. 349, pp. 701 - 721 (2019), for the Navier-Stokes problem, the main feature of the method being that the time derivative term in the subgrid-scales is not neglected. The main advantage of considering time-dependent sub-grid scales is that stable solutions for anisotropic space-time discretizations are obtained; however other benefits related with elastic problems are found along this study. Additionally, a split term-by-term stabilization method is discussed and redesigned, where only the momentum equation is approached using a term-by-term methodology, and which turns out to be much more efficient than other residual-based formulations. The proposed methods are designed for the standard and logarithmic formulations in order to deal with high Weissenberg number problems in addition to anisotropic space-time discretizations, ensuring stability in all cases. The proposed formulations are validated in several benchmarks such as the flow over a cylinder problem and the lid-driven cavity problem, obtaining stable and accurate results. A comparison between formulations and stabilization techniques is done to demonstrate the efficiency of time-dependent sub-grid scales and the term-by-term methodologies.

Keywords: Stabilized finite element methods, Variational Multiscale, Dynamic sub-grid scales, Term-by-term stabilization, Viscoelastic fluids, Log-conformation, Oldroyd-B fluid.

1 Introduction

Recent studies indicate that classical residual-based stabilized methods for unsteady incompressible flows may experience difficulties when the time step is small relative to the spatial grid size. For example, Bochev et al. [1] argue that spatial stabilization in conjunction with finite differencing in time implies destabilizing terms and that $\delta t > Ch^2$ is a sufficient condition to avoid instabilities (where δt is the time step size, C a positive constant and h the spatial grid size), although they are not conclusive about the necessity of this condition. Nevertheless, for anisotropic space-time discretizations (partitions in which h and δt are independently refined), this inequality is not necessarily satisfied [2], and in fact complications in residual-based stabilized methods are reported. These problems can happen, for instance, when small time steps result from the necessity of accuracy to solve transient problems due to the presence of non-linear terms in the differential equations, a very common issue in viscoelastic flow formulations. The results presented by Bochev et al. [3] explain why fully discrete formulations experience problems when $\delta t \rightarrow 0$, putting

the focus on the coercivity of the stabilized variational equation. These instabilities are encountered particularly in early stages of the time integration.

In particular, the approximations used in Variational Multiscale (VMS) methods [4] usually neglect the time derivative of the sub-grid scales, resulting in the inequality $\delta t > Ch^2$ being required to obtain stable solutions. Consequently, anisotropic space-time discretizations cannot guarantee stability, as it is argued by Codina et al. [5]. The sub-grid scales obtained neglecting the time derivative are denoted in [6] with the term *quasi-static*. In this sense, the work [5] results crucial, because the authors explore all the properties of the discrete formulation that is obtained when the temporal dependency of subgrid scales is accounted for. This idea, which is widely developed in the quoted paper, avoids some inconsistencies, allowing to solve turbulent flows accurately [7]. In addition, the computational effort is reduced significantly due to the reduction of non-linear iterations needed to solve at each time step.

In a more recent publication [8], the authors presents the benefits of the tracking of sub-grid scales in time for the Navier-Stokes incompressible problem using various stabilized methods, including a residual-based VMS method and a method whose structure is split term-by-term, where the use of orthogonal projections results in an optimal order non-consistent method. This work demonstrates that, considering dynamic sub-grid scales, the anisotropic time-space discretization is completely stable, i.e. the inequality $\delta t > Ch^2$ does not need to be satisfied. By following these ideas, the present work pursues to expand transient subgrid-scale methods to the viscoelastic flow problem.

The computation of viscoelastic flows leads to its own difficulties, especially when elasticity becomes dominant, i.e., when the dimensionless number known as the *Weissenberg number* is high. In these cases, the numerical instability is caused by the lack of balance between deformation rate and convection, as identified by Fattal and Kupferman [9]. The source of the so called High Weissenberg Number Problem (HWNP) is associated with the loss of positive-definiteness of the conformation tensor [4, 10], and the existence of large stress gradients and regions with high deformation rate that cause the numerical methods to fail. A new formulation was proposed by Fattal and Kupferman [10, 9] in order to deal with these shortcomings: the so called Logarithmic Conformation Representation. This formulation arises from the traditional equations of viscoelastic fluids together with a change of variables, with the objective of eliminating instabilities, allowing to extend the range of Weissenberg numbers which can be computed. In this sense, in [11] the authors apply this reformulation using a stabilized formulation based on the VMS method, which will be the basis of some of the stabilized formulations employed here.

To sum up, the purpose of the present paper is the design of stabilization techniques that allow to compute time-dependent viscoelastic flow problems with high elasticity (or Weissenberg number) and with an anisotropic space-time discretization. To achieve it, the design of a term-by-term VMS method with transient in time subgrid scales is presented. Also, along this paper both standard and logarithmic formulations are considered, compared and validated in some numerical examples.

The structure of the work is as follows: Section 2 explains the main features of the standard and logarithmic formulations in the strong and variational form for an Oldroyd-B fluid. At the end of this Section, the Galerkin finite element (FE) discretization and the time discretization are described. Once the main equations are set, Section 3 exposes the stabilized FE approach based on the VMS method considering the dynamic sub-grid scales through two different forms: the residual-based stabilization and the split term-by-term stabilization, where the particularities of the formulation design are discussed numerically. The numerical results are exposed in Section 4, where three different benchmarks are computed and analysed to validate the formulations. Finally, conclusions are collected in the last section of the work, Section 5.

2 Viscoelastic flow problem

2.1 Boundary value problem

Let us start by presenting the standard equations associated to the viscoelastic flow problem in incompressible and isothermic conditions. Let us consider a viscoelastic fluid moving in a domain Ω of \mathbb{R}^d ($d=2$ or 3), whose boundary is $\partial\Omega$, during the time interval $[0, t_f]$. The governing equations are the conservation of momentum and mass which can be expressed as

$$\rho \frac{\partial \mathbf{u}}{\partial t} + \rho \mathbf{u} \cdot \nabla \mathbf{u} - \nabla \cdot \mathbf{T} + \nabla p = \mathbf{f} \text{ in } \Omega, t \in]0, t_f[, \quad (2.1)$$

$$\nabla \cdot \mathbf{u} = 0 \text{ in } \Omega, t \in]0, t_f[, \quad (2.2)$$

where ρ denotes the constant density, $p : \Omega \times]0, t_f[\rightarrow \mathbb{R}$ is the pressure field, $\mathbf{u} : \Omega \times]0, t_f[\rightarrow \mathbb{R}^d$ is the velocity field, $\mathbf{f} : \Omega \times]0, t_f[\rightarrow \mathbb{R}^d$ is the force field and $\mathbf{T} : \Omega \times]0, t_f[\rightarrow \mathbb{R}^d \otimes \mathbb{R}^d$ is the deviatoric stress tensor. In general, \mathbf{T} is defined in terms of a viscous and a viscoelastic contribution as $\mathbf{T} = 2\eta_e \nabla^s \mathbf{u} + \boldsymbol{\sigma}$, where $\nabla^s \mathbf{u}$ is the symmetrical part of the velocity gradient and $\boldsymbol{\sigma}$ is the viscoelastic or elastic stress tensor. Note that we will write the effective (or solvent) viscosity η_e and the polymeric viscosity η_p as a function of the total viscosity η_0 , therefore, an additional parameter $\beta \in [0, 1]$ is introduced to define $\eta_e = \beta \eta_0$ and $\eta_p = (1 - \beta) \eta_0$.

To complete the system which models the viscoelastic fluid, the constitutive equation for the viscoelastic stress tensor is defined. We consider the Oldroyd-B model, which reads:

$$\frac{1}{2\eta_p} \boldsymbol{\sigma} - \nabla^s \mathbf{u} + \frac{\lambda}{2\eta_p} \left(\frac{\partial \boldsymbol{\sigma}}{\partial t} + \mathbf{u} \cdot \nabla \boldsymbol{\sigma} - \boldsymbol{\sigma} \cdot \nabla \mathbf{u} - (\nabla \mathbf{u}^T) \cdot \boldsymbol{\sigma} \right) = \mathbf{0}, \text{ in } \Omega, t \in]0, t_f[, \quad (2.3)$$

where λ is the relaxation time.

From this point, in order to distinguish operators between standard and logarithmic formulations, we employ the subscripts “std” and “log”. We define operators \mathcal{L}_{std} and \mathcal{D}_{std} , useful in the next subsections. Let us define $\mathbf{U} = [\mathbf{u}, p, \boldsymbol{\sigma}]$, $\mathbf{F}_{\text{std}} = [\mathbf{f}, 0, \mathbf{0}]$,

$$\mathcal{L}_{\text{std}}(\hat{\mathbf{u}}; \mathbf{U}) := \begin{pmatrix} -\nabla \cdot \boldsymbol{\sigma} - 2\eta_e \nabla \cdot (\nabla^s \mathbf{u}) + \rho \hat{\mathbf{u}} \cdot \nabla \mathbf{u} + \nabla p \\ \nabla \cdot \mathbf{u} \\ \frac{1}{2\eta_p} \boldsymbol{\sigma} - \nabla^s \mathbf{u} + \frac{\lambda}{2\eta_p} (\hat{\mathbf{u}} \cdot \nabla \boldsymbol{\sigma} - \boldsymbol{\sigma} \cdot \nabla \hat{\mathbf{u}} - (\nabla \hat{\mathbf{u}})^T \cdot \boldsymbol{\sigma}) \end{pmatrix} \quad (2.4)$$

and

$$\mathcal{D}_{\text{std}}(\mathbf{U}) := \begin{pmatrix} \rho \frac{\partial \mathbf{u}}{\partial t} \\ 0 \\ \frac{\lambda}{2\eta_p} \left(\frac{\partial \boldsymbol{\sigma}}{\partial t} \right) \end{pmatrix}.$$

As a consequence, equations (2.1), (2.2) and (2.3) can be rewritten, considering $\mathcal{D}_t = \mathcal{D}_{\text{std}}$, $\mathcal{L} = \mathcal{L}_{\text{std}}$ and $\mathbf{F} = \mathbf{F}_{\text{std}}$, as:

$$\mathcal{D}_t(\mathbf{U}) + \mathcal{L}(\mathbf{u}; \mathbf{U}) = \mathbf{F}. \quad (2.5)$$

Finally, we need to define the boundary conditions that close the problem. For simplicity, $\mathbf{u} = \mathbf{0}$ on $\partial\Omega$ is considered. In the case of boundary conditions for the elastic stresses, in principle they do not need to be prescribed, but enforcing them allows to save computational time sometimes. On the other hand, they can be fixed only on the inflow boundary, $\Gamma_{\text{in}} = \{\mathbf{x} \in \partial\Omega \mid (\mathbf{u} \cdot \mathbf{n})(\mathbf{x}) < 0\}$, where \mathbf{n} is the outward unit normal vector to $\partial\Omega$. The problem is completed with the initial conditions for velocity and elastic stress

($\mathbf{u} = \mathbf{u}^0$ and $\boldsymbol{\sigma} = \boldsymbol{\sigma}^0$) at time $t = 0$, being \mathbf{u}^0 and $\boldsymbol{\sigma}^0$ functions defined in the whole domain Ω .

We will now briefly describe the viscoelastic equations when the logarithmic reformulation is considered. Note that the complete development employed is extensively explained in [11]. The reformulation is derived basically from a change of variables, where the stress tensor is replaced by $\boldsymbol{\sigma} = \frac{\eta_p}{\lambda_0}(\boldsymbol{\tau} - \mathbf{I})$, and in turn, the conformation tensor $\boldsymbol{\tau}$ is written as $\boldsymbol{\tau} = \exp(\psi)$ in (2.1), (2.2) and (2.3). Particularly, λ_0 is linearly dependent with λ and is defined as $\lambda_0 = \max\{k\lambda, \lambda_{0,\min}\}$, being k a constant and $\lambda_{0,\min}$ a given threshold. Therefore, the new equations of the logarithmic conformation formulation are expressed as follows:

$$\rho \frac{\partial \mathbf{u}}{\partial t} - \frac{\eta_p}{\lambda_0} \nabla \cdot \exp(\psi) - 2\eta_e \nabla \cdot (\nabla^s \mathbf{u}) + \rho \mathbf{u} \cdot \nabla \mathbf{u} + \nabla p = \mathbf{f}, \quad (2.6)$$

$$\nabla \cdot \mathbf{u} = 0, \quad (2.7)$$

$$\begin{aligned} & \frac{1}{2\lambda_0}(\exp(\psi) - \mathbf{I}) - \nabla^s \mathbf{u} \\ & + \frac{\lambda}{2\lambda_0} \left(\frac{\partial \exp(\psi)}{\partial t} + \mathbf{u} \cdot \nabla \exp(\psi) - \exp(\psi) \cdot \nabla \mathbf{u} - (\nabla \mathbf{u})^T \cdot \exp(\psi) + 2\nabla^s \mathbf{u} \right) = \mathbf{0}, \end{aligned} \quad (2.8)$$

where the unknowns are the velocity, the pressure, and tensor ψ that depends directly on the viscoelastic stress tensor $\boldsymbol{\sigma}$.

Analogously to what was done for the standard formulation, calling $\mathbf{U} = [\mathbf{u}, p, \psi]$, $\mathbf{F}_{\log} = [\mathbf{f}, 0, \frac{1}{2\lambda_0} \mathbf{I}]$,

$$\mathcal{L}_{\log}(\hat{\mathbf{u}}; \mathbf{U}) := \begin{pmatrix} -\frac{\eta_p}{\lambda_0} \nabla \cdot (\exp(\psi)) - 2\eta_e \nabla \cdot (\nabla^s \mathbf{u}) + \rho \hat{\mathbf{u}} \cdot \nabla \mathbf{u} + \nabla p \\ \nabla \cdot \mathbf{u} \\ \frac{1}{2\lambda_0} \exp(\psi) - \nabla^s \mathbf{u} + \frac{\lambda}{2\lambda_0} (\hat{\mathbf{u}} \cdot \nabla (\exp(\psi))) \\ -\exp(\psi) \cdot \nabla \hat{\mathbf{u}} - (\nabla \hat{\mathbf{u}})^T \cdot \exp(\psi) + 2\nabla^s \mathbf{u} \end{pmatrix} \quad (2.9)$$

and

$$\mathcal{D}_{\log}(\mathbf{U}) := \begin{pmatrix} \rho \frac{\partial \mathbf{u}}{\partial t} \\ 0 \\ \frac{\lambda}{2\lambda_0} \frac{\partial \exp(\psi)}{\partial t} \end{pmatrix},$$

equations (2.6)-(2.8) can be expressed as equation (2.5), where $\mathcal{D}_t = \mathcal{D}_{\log}$, $\mathcal{L} = \mathcal{L}_{\log}$ and $\mathbf{F} = \mathbf{F}_{\log}$. Similar considerations can be done for this formulation referring to the boundary conditions. In this case tensor ψ is not prescribed, similarly to what is done with the elastic stresses $\boldsymbol{\sigma}$ in the standard formulation.

2.2 Variational form

Let us introduce some specific notation in order to define the weak form of the viscoelastic problem:

- The space of square integrable functions in a domain ω is denoted by $L^2(\omega)$, and the space of functions whose distributional derivatives of order up to $m \geq 0$ (integer) belong to $L^2(\omega)$ is denoted by $H^m(\omega)$.
- The space $H_0^1(\omega)$ comprises functions in $H^1(\omega)$ vanishing on $\partial\omega$.
- The topological dual of $H_0^1(\Omega)$ is denoted by $H^{-1}(\Omega)$, the duality pairing being $\langle \cdot, \cdot \rangle$.

- The L^2 inner product in ω (for scalars, vectors and tensors) is denoted by $(\cdot, \cdot)_\omega$ and the integral over ω of the product of two general functions is written as $\langle \cdot, \cdot \rangle_\omega$, the subscript being omitted when $\omega = \Omega$.
- The norm in a space X is denoted by $\|\cdot\|_X$, except in the case $X = L^2(\Omega)$, where the subscript is omitted.

Using this notation, the stress, velocity and pressure spaces for the continuous standard problem can be taken as $\boldsymbol{\Upsilon} = H^1(\Omega)^{d \times d}_{\text{sym}}$ (symmetric second order tensor with components in $H^1(\Omega)$), $\mathbf{V}_0 = H_0^1(\Omega)^d$ and $\mathcal{Q} = L^2(\Omega)/\mathbb{R}$, respectively, for each fixed time t (the regularity for the stress space could be relaxed).

The weak form of the problem consists in finding $\mathbf{U} = [\mathbf{u}, p, \boldsymbol{\sigma}] :]0, t_f[\rightarrow \mathbf{X} := \mathbf{V}_0 \times \mathcal{Q} \times \boldsymbol{\Upsilon}$, such that the initial conditions are satisfied and:

$$\begin{aligned} \left(\rho \frac{\partial \mathbf{u}}{\partial t}, \mathbf{v} \right) + (\boldsymbol{\sigma}, \nabla^s \mathbf{v}) + 2(\eta_e \nabla^s \mathbf{u}, \nabla^s \mathbf{v}) + \langle \rho \mathbf{u} \cdot \nabla \mathbf{u}, \mathbf{v} \rangle - (p, \nabla \cdot \mathbf{v}) &= \langle \mathbf{f}, \mathbf{v} \rangle, \\ (q, \nabla \cdot \mathbf{u}) &= 0, \\ \frac{1}{2\eta_p} (\boldsymbol{\sigma}, \chi) - (\nabla^s \mathbf{u}, \chi) + \frac{\lambda}{2\eta_p} \left(\frac{\partial \boldsymbol{\sigma}}{\partial t} + \mathbf{u} \cdot \nabla \boldsymbol{\sigma} - \boldsymbol{\sigma} \cdot \nabla \mathbf{u} - (\nabla \mathbf{u})^T \cdot \boldsymbol{\sigma}, \chi \right) &= 0, \end{aligned}$$

for all $\mathbf{V} = [\mathbf{v}, q, \chi] \in \mathbf{X}$, where it is assumed that \mathbf{f} is such that $\langle \mathbf{f}, \mathbf{v} \rangle$ is well defined. In compact form, the problem can be written as:

$$\mathcal{G}_{\text{std}}(\mathbf{U}, \mathbf{V}) + B_{\text{std}}(\mathbf{u}; \mathbf{U}, \mathbf{V}) = L_{\text{std}}(\mathbf{V}), \quad (2.10)$$

for all $\mathbf{V} \in \mathbf{X}$, where

$$\mathcal{G}_{\text{std}}(\mathbf{U}, \mathbf{V}) = \left(\rho \frac{\partial \mathbf{u}}{\partial t}, \mathbf{v} \right) + \frac{\lambda}{2\eta_p} \left(\frac{\partial \boldsymbol{\sigma}}{\partial t}, \chi \right), \quad (2.11)$$

$$\begin{aligned} B_{\text{std}}(\hat{\mathbf{u}}; \mathbf{U}, \mathbf{V}) &= 2\eta_e (\nabla^s \mathbf{u}, \mathbf{v}) + \langle \rho \hat{\mathbf{u}} \cdot \nabla \mathbf{u}, \mathbf{v} \rangle + (\boldsymbol{\sigma}, \nabla^s \mathbf{v}) \\ &\quad - (p, \nabla \cdot \mathbf{v}) + (q, \nabla \cdot \mathbf{u}) + \frac{1}{2\eta_p} (\boldsymbol{\sigma}, \chi) - (\nabla^s \mathbf{u}, \chi) \\ &\quad + \frac{\lambda}{2\eta_p} (\hat{\mathbf{u}} \cdot \nabla \boldsymbol{\sigma} - \boldsymbol{\sigma} \cdot \nabla \hat{\mathbf{u}} - (\nabla \hat{\mathbf{u}})^T \cdot \boldsymbol{\sigma}, \chi), \end{aligned} \quad (2.12)$$

$$L_{\text{std}}(\mathbf{V}) = \langle \mathbf{f}, \mathbf{v} \rangle. \quad (2.13)$$

Considering now the logarithmic reformulation of the viscoelastic flow problem, the spaces for the velocity and pressure for the continuous problems are the ones defined above for the standard formulation, and now, the space for tensor $\boldsymbol{\psi}$ is denoted by $\bar{\boldsymbol{\Upsilon}}$ for each fixed time t , where an appropriate regularity is assumed.

The weak form of the problem consists in finding $\mathbf{U} = [\mathbf{u}, p, \boldsymbol{\psi}] :]0, t_f[\rightarrow \bar{\mathbf{X}} := \mathbf{V}_0 \times \mathcal{Q} \times \bar{\boldsymbol{\Upsilon}}$, such that the initial conditions are satisfied and:

$$\begin{aligned} \left(\rho \frac{\partial \mathbf{u}}{\partial t}, \mathbf{v} \right) + \frac{\eta_p}{\lambda_0} (\exp(\boldsymbol{\psi}), \nabla^s \mathbf{v}) + 2(\eta_e \nabla^s \mathbf{u}, \nabla^s \mathbf{v}) \\ + \langle \rho \mathbf{u} \cdot \nabla \mathbf{u}, \mathbf{v} \rangle - (p, \nabla \cdot \mathbf{v}) &= \langle \mathbf{f}, \mathbf{v} \rangle, \end{aligned} \quad (2.14)$$

$$(q, \nabla \cdot \mathbf{u}) = 0, \quad (2.15)$$

$$\begin{aligned} \frac{1}{2\lambda_0} (\exp(\boldsymbol{\psi}), \chi) - (\nabla^s \mathbf{u}, \chi) + \frac{\lambda}{2\lambda_0} \left(\frac{\partial \exp(\boldsymbol{\psi})}{\partial t}, \chi \right) \\ + \frac{\lambda}{2\lambda_0} (\mathbf{u} \cdot \nabla \exp(\boldsymbol{\psi}), \chi) \\ + \frac{\lambda}{2\lambda_0} (-\exp(\boldsymbol{\psi}) \cdot \nabla \mathbf{u} - (\nabla \mathbf{u})^T \cdot \exp(\boldsymbol{\psi}) + 2\nabla^s \mathbf{u}, \chi) &= \frac{1}{2\lambda_0} \langle \mathbf{I}, \chi \rangle, \end{aligned} \quad (2.16)$$

for all $\mathbf{V} = [\mathbf{v}, q, \chi] \in \mathcal{X}$. Again taking into account the new definition of \mathbf{U} for this formulation, the problem can be written as:

$$\mathcal{G}_{\log}(\mathbf{U}, \mathbf{V}) + B_{\log}(\mathbf{u}; \mathbf{U}, \mathbf{V}) = L_{\log}(\mathbf{V}), \quad (2.17)$$

where each term is defined as

$$\mathcal{G}_{\log}(\mathbf{U}, \mathbf{V}) = \left(\rho \frac{\partial \mathbf{u}}{\partial t}, \mathbf{v} \right) + \frac{\lambda}{2\lambda_0} \left(\frac{\partial \exp(\psi)}{\partial t}, \chi \right), \quad (2.18)$$

$$\begin{aligned} B_{\log}(\hat{\mathbf{u}}; \mathbf{U}, \mathbf{V}) &= \frac{\eta_p}{\lambda_0} (\exp(\psi), \nabla^s \mathbf{v}) + 2(\eta_e \nabla^s \mathbf{u}, \nabla^s \mathbf{v}) + \langle \rho \hat{\mathbf{u}} \cdot \nabla \mathbf{u}, \mathbf{v} \rangle - (p, \nabla \cdot \mathbf{v}) \\ &\quad + (\nabla \cdot \mathbf{u}, q) + \frac{1}{2\lambda_0} (\exp(\psi), \chi) - (\nabla^s \mathbf{u}, \chi) \\ &\quad + \frac{\lambda}{2\lambda_0} (\mathbf{u} \cdot \nabla \exp(\psi) - \exp(\psi) \cdot \nabla \mathbf{u} - (\nabla \mathbf{u})^T \cdot \exp(\psi) + 2\nabla^s \mathbf{u}, \chi), \end{aligned} \quad (2.19)$$

$$L_{\log}(\mathbf{V}) = \langle \mathbf{f}, \mathbf{v} \rangle + \frac{1}{2\lambda_0} \langle \mathbf{I}, \chi \rangle. \quad (2.20)$$

2.3 Galerkin finite element discretization and time discretization

The standard Galerkin approximation for the variational problem in both formulations (standard and logarithmic), which have been established in (2.10) and (2.17), is described next. Let $\mathcal{T}_h = \{K\}$ be a finite element partition of the domain Ω . The diameter of an element $K \in \mathcal{T}_h$ is denoted by h_K and the diameter of the partition is defined as $h = \max\{h_K | K \in \mathcal{T}_h\}$.

In the case of the standard formulation, from \mathcal{T}_h we may construct conforming finite element spaces for the velocity, the pressure and the elastic stress, $\mathcal{V}_h \subset \mathcal{V}$, $\mathcal{Q}_h \subset \mathcal{Q}$, $\mathbf{T}_h \subset \mathbf{T}$, respectively. Calling $\mathcal{X}_h := \mathcal{V}_h \times \mathcal{Q}_h \times \mathbf{T}_h$ the Galerkin FE approximation of the problem consists in finding $\mathbf{U}_h : [0, t_f] \rightarrow \mathcal{X}_h$, such that:

$$\mathcal{G}_{\text{std}}(\mathbf{U}_h, \mathbf{V}_h) + B_{\text{std}}(\mathbf{u}_h; \mathbf{U}_h, \mathbf{V}_h) = \mathbf{F}_{\text{std}}(\mathbf{V}_h),$$

for all $\mathbf{V}_h = [\mathbf{v}_h, q_h, \chi_h] \in \mathcal{X}_h$, and satisfying the appropriate initial conditions.

On the other hand, for the logarithmic conformation reformulation, from \mathcal{T}_h we construct the finite element space for the new variable ψ , $\bar{\mathbf{T}}_h \subset \bar{\mathbf{T}}$. So, $\bar{\mathcal{X}}_h := \mathcal{V}_h \times \mathcal{Q}_h \times \bar{\mathbf{T}}_h$ is the Galerkin FE now now, and the Galerkin approximation consists in finding $\mathbf{U}_h : [0, t_f] \rightarrow \bar{\mathcal{X}}_h$, such that

$$\mathcal{G}_{\log}(\mathbf{U}_h, \mathbf{V}_h) + B_{\log}(\mathbf{u}_h; \mathbf{U}_h, \mathbf{V}_h) = \mathbf{F}_{\log}(\mathbf{V}_h),$$

for all $\mathbf{V}_h = [\mathbf{v}_h, q_h, \chi_h] \in \mathcal{X}_h$.

It is well known that the Galerkin approximation is unstable unless convective terms are not relevant and appropriate compatibility conditions between \mathcal{Q}_h and \mathcal{V}_h , on the one hand, and between \mathcal{V}_h and \mathbf{T}_h , on the other hand, are met (see for example [12] and references therein). In the next Section we will present a stable formulation, able in particular to deal with continuous approximations for all fields, which is the situation we shall consider.

We define now the discretization in time. Consider a partition of the interval $[0, t_f]$ in δt constant size time steps, and let $t^n = n\delta t$, being $n = 0, 1, 2, \dots$. Let $f(t)$ be a generic time dependent function. We will denote as f^n the approximation of the function at time level t^n . A backward differencing (BDF) approximation to the time derivative of function f of order $k = 1, 2, \dots$, is given by $\frac{\delta_k f^{n+1}}{\delta t}$, where $\delta_k f^{n+1}$ is defined as

$$\delta_k f^{n+1} = \frac{1}{\gamma_k} \left(f^{n+1} - \sum_{i=0}^{k-1} \varphi_k^i f^{n-i} \right),$$

and γ_k and φ_k^i are numerical parameters. Particularly, first and second order backward differencing schemes (respectively referenced as BDF1 and BDF2) have been implemented in this work, based on the approximations:

$$\begin{aligned}\frac{\delta_1 f^{n+1}}{\delta t} &= \frac{f^{n+1} - f^n}{\delta t} = \left. \frac{\partial f}{\partial t} \right|_{t^{n+1}} + \mathcal{O}(\delta t), \\ \frac{\delta_2 f^{n+1}}{\delta t} &= \frac{3f^{n+1} - 4f^n + f^{n-1}}{2\delta t} = \left. \frac{\partial f}{\partial t} \right|_{t^{n+1}} + \mathcal{O}(\delta t^2).\end{aligned}$$

In any case, the stabilized finite element method which will be exposed is independent of the time scheme used.

For the logarithmic formulation, using the approximations of the exponential described in [11], we obtain the next expression for the *linearized* time derivative of the exponential:

$$\begin{aligned}\left. \frac{\partial(\exp(\psi))}{\partial t} \right|_{t^{n+1}} &= \frac{1}{\delta t \gamma_k} \left[\exp(\hat{\psi}^{n+1}) \cdot \psi^{n+1} + \exp(\hat{\psi}^{n+1}) - \exp(\hat{\psi}^{n+1}) \cdot \hat{\psi}^{n+1} \right. \\ &\quad \left. - \sum_{i=0}^{k-1} \varphi_k^i \exp(\psi^{n-i}) \right] + \mathcal{O}(\delta t^k) + \mathcal{O}((\delta \psi^{n+1})^2),\end{aligned}$$

where $\hat{\psi}^{n+1}$ stands for a previous guess of ψ^{n+1} that depends on the linearization scheme and $\delta \psi^{n+1} = \psi^{n+1} - \hat{\psi}^{n+1}$.

3 Stabilized finite element formulation

In this section, two different stabilized finite element methods for computing viscoelastic flows will be presented: the first is purely based on the finite element residual, and the second one is a term-by-term method. However, both depart from the framework described in [4], which consists in splitting the unknowns \mathbf{U} in the sum of two components, \mathbf{U}_h (component which can be captured by the finite element space) and $\tilde{\mathbf{U}}$ (the remainder, called sub-grid scale). For more details about this development, see [13]. Additionally, we will develop these methods for the two different formulations considered in this work: the well-known standard viscoelastic formulation and for the logarithmic reformulation. Note that the stabilization methods proposed are suitable for the three field Newtonian problem too, which is recovered by considering the parameter λ equal to zero.

3.1 Residual-based VMS methods

The problem that we pretend to approximate is (2.5) in strong form for both standard (2.10) and logarithmic (2.17) formulations.

Firstly, we will deal with the standard formulation. Let us suppose that $\mathcal{L}_{\text{std}}(\hat{\mathbf{u}}; \cdot)$ is a linear operator for a given $\hat{\mathbf{u}}$. Introducing the sub-grid scale decomposition and integrating by parts, the method leads to find $\mathbf{U}_h :]0, t_f[\rightarrow \mathcal{X}_h$ such that

$$\mathcal{G}_{\text{std}}(\mathbf{U}_h, \mathbf{V}_h) + B_{\text{std}}(\mathbf{u}_h; \mathbf{U}_h, \mathbf{V}_h) + \sum_K \langle \tilde{\mathbf{U}}, \mathcal{L}^*(\mathbf{u}_h; \mathbf{V}_h) \rangle_K = L_{\text{std}}(\mathbf{V}), \quad (3.1)$$

for all $\mathbf{V}_h \in \mathcal{X}_h$, where $\mathcal{L}^*(\mathbf{u}_h; \mathbf{V}_h)$ is the formal adjoint of the operator of $\mathcal{L}_{\text{std}}(\hat{\mathbf{u}}; \cdot)$, typically without considering boundary conditions, $\tilde{\mathbf{U}}$ is the sub-grid scale, which needs to be approximated and has components $\tilde{\mathbf{U}} = [\tilde{\mathbf{u}}, \tilde{p}, \tilde{\boldsymbol{\sigma}}]$. To justify (3.1), see e.g. [14], and recall that we are considering all approximations continuous.

Analogously, for the logarithmic formulation, method leads to find $\mathbf{U}_h :]0, t_f[\rightarrow \bar{\mathcal{X}}_h$ such that

$$\mathcal{G}_{\log}(\mathbf{U}_h, \mathbf{V}_h) + B_{\log}(\mathbf{u}_h; \mathbf{U}_h, \mathbf{V}_h) + \sum_K \langle \tilde{\mathbf{U}}, \mathcal{L}^*(\mathbf{u}_h; \mathbf{V}_h) \rangle_K = L_{\log}(\mathbf{V}), \quad (3.2)$$

for all $\mathbf{V}_h \in \mathcal{X}_h$. Let us remark that for both formulations (standard and logarithmic) the same operator $\mathcal{L}^*(\hat{\mathbf{u}}; \cdot)$ will be employed, following the process described in [11]:

$$\mathcal{L}^*(\hat{\mathbf{u}}; \mathbf{V}) := \begin{pmatrix} \nabla \cdot \boldsymbol{\chi} - 2\eta_e \nabla \cdot (\nabla^s \mathbf{v}) - \rho \hat{\mathbf{u}} \cdot \nabla \mathbf{v} - \nabla q \\ -\nabla \cdot \mathbf{v} \\ \frac{1}{2\eta_p} \boldsymbol{\chi} + \nabla^s \mathbf{v} - \frac{\lambda}{2\eta_p} (\hat{\mathbf{u}} \cdot \nabla \boldsymbol{\chi} + \boldsymbol{\chi} \cdot (\nabla \hat{\mathbf{u}})^T + \nabla \hat{\mathbf{u}} \cdot \boldsymbol{\chi}) \end{pmatrix}.$$

This is due to the fact that we have not changed variables in the stress test function.

Once operators \mathcal{D}_t and \mathcal{L} are defined for both formulations, the sub-grid scales can be written in terms of the finite element component as

$$\frac{\partial \tilde{\mathbf{U}}}{\partial t} + \boldsymbol{\alpha}^{-1} \tilde{\mathbf{U}} = \tilde{P} [\mathbf{F} - \mathcal{D}_t(\mathbf{U}_h) - \mathcal{L}(\mathbf{u}_h; \mathbf{U}_h)], \quad (3.3)$$

where we denote \tilde{P} as the L^2 projection onto the space of sub-grid scales.

Note that the most classical approach, the Algebraic Sub-Grid Scale (ASGS) method is recovered if \tilde{P} is the projection onto the space of FE residuals. On the contrary, if \tilde{P} is taken as the orthogonal projection to the FE space, the Orthogonal Sub-Scale Stabilization (OSGS) method [15] is recovered. On the other hand, $\boldsymbol{\alpha}$ is taken as a diagonal matrix of stabilization parameters, $\boldsymbol{\alpha} = \text{diag}(\alpha_1 \mathbf{I}_d, \alpha_2, \alpha_3 \mathbf{I}_{d \times d})$, with \mathbf{I}_d the identity on vectors of \mathbb{R}^d , $\mathbf{I}_{d \times d}$ the identity on second order tensors, and parameters α_i , $i = 1, 2, 3$, being defined as in [12]:

$$\alpha_1 = \left[c_1 \frac{\eta_0}{h_1^2} + c_2 \frac{\rho |\mathbf{u}_h|}{h_2} \right]^{-1}, \quad (3.4)$$

$$\alpha_2 = \frac{h_1^2}{c_1 \alpha_1}, \quad (3.5)$$

$$\alpha_3 = \left[c_3 \frac{1}{2\eta_p} + c_4 \left(\frac{\lambda}{2\eta_p} \frac{|\mathbf{u}_h|}{h_2} + \frac{\lambda}{\eta_p} |\nabla \mathbf{u}_h| \right) \right]^{-1}, \quad (3.6)$$

where c_1, c_2, c_3 and c_4 are constants, h_1 is the characteristic length calculated as the square root of the element area in the two-dimensional case and the cubic root of the element volume in the three-dimensional case, and h_2 is another characteristic length calculated as the element length in the streamline direction. Term $|\mathbf{u}_h|$ is the Euclidean norm of the velocity and $|\nabla \mathbf{u}_h|$ is the Frobenius norm of the velocity gradient.

Now, inserting the solution of (3.3) with $\boldsymbol{\alpha}$ given by (3.4)-(3.6) into (3.1), we obtain the following residual-based stabilization method: find $\mathbf{U}_h :]0, t_f[\rightarrow \mathcal{X}_h$ such that

$$\begin{aligned} & \mathcal{G}_{\text{std}}(\mathbf{U}_h, \mathbf{V}_h) + B_{\text{std}}(\mathbf{u}_h; \mathbf{U}_h, \mathbf{V}_h) + \sum_K \langle \tilde{p}, -\nabla \cdot \mathbf{v}_h \rangle_K \\ & + \sum_K \langle \tilde{\mathbf{u}}, \nabla \cdot \boldsymbol{\chi}_h - 2\eta_e \nabla \cdot (\nabla^s \mathbf{v}_h) - \rho \mathbf{u}_h \cdot \nabla \mathbf{v}_h - \nabla q_h \rangle_K \\ & + \sum_K \left\langle \tilde{\boldsymbol{\sigma}}, \frac{1}{2\eta_p} \boldsymbol{\chi}_h + \nabla^s \mathbf{v}_h - \frac{\lambda}{2\eta_p} \langle \mathbf{u}_h \cdot \nabla \boldsymbol{\chi}_h + \boldsymbol{\chi}_h \cdot (\nabla \mathbf{u}_h)^T + \nabla \mathbf{u}_h \cdot \boldsymbol{\chi}_h \rangle \right\rangle_K \\ & = \langle \mathbf{f}, \mathbf{v}_h \rangle, \end{aligned} \quad (3.7)$$

where $\tilde{\mathbf{u}}$, \tilde{p} and $\tilde{\boldsymbol{\sigma}}$ are the sub-grid scales of the momentum, the continuity and the constitutive equation, respectively, and $B_{\text{std}}(\hat{\mathbf{u}}_h; \mathbf{U}_h, \mathbf{V}_h)$ is given in (2.12).

The sub-grid scales are the solution to the problem:

$$\rho \frac{\partial \tilde{\mathbf{u}}}{\partial t} + \alpha_1^{-1} \tilde{\mathbf{u}} = \tilde{P} \left(\mathbf{f} - \left(\rho \frac{\partial \mathbf{u}_h}{\partial t} - \nabla \cdot \boldsymbol{\sigma}_h - 2\eta_e \nabla \cdot (\nabla^s \mathbf{u}_h) + \rho \mathbf{u}_h \cdot \nabla \mathbf{u}_h + \nabla p_h \right) \right), \quad (3.8)$$

$$\alpha_2^{-1} \tilde{p} = -\tilde{P}(\nabla \cdot \mathbf{u}_h), \quad (3.9)$$

$$\begin{aligned} \frac{\lambda}{2\eta_p} \frac{\partial \tilde{\boldsymbol{\sigma}}}{\partial t} + \alpha_3^{-1} \tilde{\boldsymbol{\sigma}} &= \tilde{P} \left(-\frac{1}{2\eta_p} \boldsymbol{\sigma}_h + \nabla^s \mathbf{u}_h \right) \\ &\quad + \tilde{P} \left(-\frac{\lambda}{2\eta_p} \left(\frac{\partial \boldsymbol{\sigma}_h}{\partial t} + \mathbf{u}_h \cdot \nabla \boldsymbol{\sigma}_h - \boldsymbol{\sigma}_h \cdot \nabla \mathbf{u}_h - (\nabla \mathbf{u}_h)^T \cdot \boldsymbol{\sigma}_h \right) \right). \end{aligned} \quad (3.10)$$

Note that the stabilization terms added to the Galerkin method in (3.7) are proportional to the finite element residuals of the momentum, the continuity and the constitutive equation. Due to this, the stabilized method defined by (3.7) will be denoted as a residual-based VMS method. Furthermore the prefix *orthogonal* will be added if $\tilde{P} = P_h^\perp$.

On the other hand, if the time derivatives of the velocity sub-grid scale (in equation (3.8)) and the stress sub-grid scale (in equation (3.10)) are neglected, the method is usually called *quasi-static*, otherwise it will be denoted as *dynamic*. Particularly, when $\tilde{P} = P_h^\perp$, two additional simplifications can be done:

1. $P_h^\perp \left(\frac{\partial \mathbf{u}_h}{\partial t} \right) = 0$ and $P_h^\perp \left(\frac{\partial \boldsymbol{\sigma}_h}{\partial t} \right) = 0$.
2. $P_h^\perp(\mathbf{f}) \approx 0$.

If these approximations are adopted, a weakly consistent method is obtained, although if \mathbf{f} is a finite element function, full consistency is recovered. The initial condition for the velocity and stress sub-grid scales in (3.8) and (3.10) can be taken as zero [16].

For the logarithmic reformulation, equation (3.2), considering the expression of the sub-grid scales (3.3) it can be expressed as

$$\begin{aligned} \mathcal{G}_{\log}(\mathbf{U}_h, \mathbf{V}_h) + B_{\log}(\mathbf{u}_h; \mathbf{U}_h, \mathbf{V}_h) &+ \sum_K \langle \tilde{\mathbf{u}}, \nabla \cdot \boldsymbol{\chi}_h - 2\eta_e \nabla \cdot (\nabla^s \mathbf{v}_h) - \rho \mathbf{u}_h \cdot \nabla \mathbf{v}_h - \nabla q_h \rangle_K \\ &+ \sum_K \langle \tilde{p}, -\nabla \cdot \mathbf{v}_h \rangle_K + \sum_K \left\langle \tilde{\boldsymbol{\sigma}}, \frac{1}{2\eta_p} \boldsymbol{\chi}_h + \nabla^s \mathbf{v}_h \right\rangle_K \\ &+ \sum_K \left\langle \tilde{\boldsymbol{\sigma}}, -\frac{\lambda}{2\eta_p} (\boldsymbol{\chi}_h \cdot (\nabla \mathbf{u}_h)^T + \nabla \mathbf{u}_h \cdot \boldsymbol{\chi}_h) \right\rangle_K \\ &= \langle \mathbf{f}, \mathbf{v}_h \rangle + \frac{1}{2\lambda_0} \langle \mathbf{I}, \boldsymbol{\chi} \rangle, \end{aligned}$$

where $\tilde{\mathbf{u}}$, \tilde{p} and $\tilde{\boldsymbol{\psi}}$ are the sub-grid scales of the momentum, the continuity and the constitutive equation respectively, and B_{\log} is the bilinear form of the problem when the logarithmic formulation is considered. We have to remark that the sub-grid scale of the constitutive equation, for simplicity, has also been computed as $\tilde{\boldsymbol{\sigma}}$ in the logarithmic case, considering $\tilde{\boldsymbol{\sigma}} = \frac{\eta_p}{\lambda_0} (\exp(\tilde{\boldsymbol{\psi}}) - \mathbf{I})$. As a residual-based VMS method is applied, sub-grid scales are defined as follows:

$$\begin{aligned} \rho \frac{\partial \tilde{\mathbf{u}}}{\partial t} + \alpha_1^{-1} \tilde{\mathbf{u}} &= \tilde{P} \left(\mathbf{f} - \left(\rho \frac{\partial \mathbf{u}_h}{\partial t} - \frac{\eta_p}{\lambda_0} \nabla \cdot \exp(\boldsymbol{\psi}_h) \right) \right) \\ &\quad + \tilde{P} (-2\eta_e \nabla \cdot (\nabla^s \mathbf{u}_h) + \rho \mathbf{u}_h \cdot \nabla \mathbf{u}_h + \nabla p_h), \end{aligned} \quad (3.11)$$

$$\alpha_2^{-1} \tilde{p} = \tilde{P} (-\nabla \cdot \mathbf{u}_h), \quad (3.12)$$

$$\begin{aligned} \frac{\lambda}{2\eta_p} \frac{\partial \tilde{\boldsymbol{\sigma}}}{\partial t} + \alpha_3^{-1} \tilde{\boldsymbol{\sigma}} &= \tilde{P} \left(-\frac{1}{2\lambda_0} \exp(\boldsymbol{\psi}_h) + \nabla^s \mathbf{u}_h \right) \\ &\quad + \tilde{P} \left(-\frac{\lambda}{2\lambda_0} \left(\frac{\partial \exp(\boldsymbol{\psi}_h)}{\partial t} + \mathbf{u}_h \cdot \nabla (\exp(\boldsymbol{\psi}_h)) \right) \right) \end{aligned}$$

$$\begin{aligned}
& + \tilde{P} \left(-\frac{\lambda}{2\lambda_0} (-\exp(\psi_h) \cdot \nabla \mathbf{u}_h) \right) \\
& + \tilde{P} \left(-\frac{\lambda}{2\lambda_0} ((\nabla \mathbf{u}_h)^T \cdot \exp(\psi_h) + 2\nabla^s \mathbf{u}_h) \right). \tag{3.13}
\end{aligned}$$

Note that the stabilized parameters $\boldsymbol{\alpha}$ are the same as those defined by the standard formulation (3.4)-(3.6).

3.2 Term-by-term stabilized formulation

3.2.1 Motivation

The method proposed here has been motivated by the fact that not all the terms of the product of $\nabla \cdot \boldsymbol{\chi}_h - 2\eta_e \nabla \cdot (\nabla^s \mathbf{v}_h) - \rho \mathbf{u}_h \cdot \nabla \mathbf{v}_h - \nabla q_h$, and the terms that contribute to $\tilde{\mathbf{u}}$ in (3.7) provide stability. Likewise, the same occurs for the constitutive equation adjoint,

$$\frac{1}{2\eta_p} \boldsymbol{\chi}_h + \nabla^s \mathbf{v}_h - \frac{\lambda}{2\eta_p} (\mathbf{u}_h \cdot \nabla \boldsymbol{\chi}_h + \boldsymbol{\chi}_h \cdot (\nabla \mathbf{u}_h)^T + \nabla \mathbf{u}_h \cdot \boldsymbol{\chi}_h),$$

and terms of $\tilde{\boldsymbol{\sigma}}$. Therefore, some of these terms can be neglected without loss of stability. This is the key idea in term-by-term stabilization methods (developed, for example in [17, 18, 13]).

Let us consider the expresions (3.8) and (3.10), taking into account that $\tilde{P} = P_h^\perp$, $P_h^\perp(\mathbf{f}) \approx \mathbf{0}$, $P_h^\perp\left(\frac{\partial \mathbf{u}_h}{\partial t}\right) = 0$ and $P_h^\perp\left(\frac{\partial \boldsymbol{\sigma}_h}{\partial t}\right) = 0$. Therefore we can rewrite them as follows:

$$\begin{aligned}
\rho \frac{\partial \tilde{\mathbf{u}}}{\partial t} + \alpha_1^{-1} \tilde{\mathbf{u}} &= P_h^\perp (\nabla \cdot \boldsymbol{\sigma}_h) + P_h^\perp (2\eta_e \nabla \cdot (\nabla^s \mathbf{u}_h)) - P_h^\perp (\rho \mathbf{u}_h \cdot \nabla \mathbf{u}_h) - P_h^\perp (\nabla p_h), \tag{3.14}
\end{aligned}$$

$$\begin{aligned}
\frac{\lambda}{2\eta_p} \frac{\partial \tilde{\boldsymbol{\sigma}}}{\partial t} + \alpha_3^{-1} \tilde{\boldsymbol{\sigma}} &= -P_h^\perp \left(\frac{1}{2\eta_p} \boldsymbol{\sigma}_h \right) + P_h^\perp (\nabla^s \mathbf{u}_h) \\
&\quad - P_h^\perp \left(\frac{\lambda}{2\eta_p} \mathbf{u}_h \cdot \nabla \boldsymbol{\sigma}_h \right) + P_h^\perp \left(\frac{\lambda}{2\eta_p} (\boldsymbol{\sigma}_h \cdot \nabla \mathbf{u}_h + (\nabla \mathbf{u}_h)^T \cdot \boldsymbol{\sigma}_h) \right). \tag{3.15}
\end{aligned}$$

The key ingredient that allows to consider any of these terms instead the residual based VMS is the orthogonal projection P_h^\perp . The right-hand-side (RHS) of (3.14) and (3.15) is not zero when the FE solution is replaced by the continuous solution, and consequently the method is not consistent. Nevertheless, the consistency error is optimal [19].

Additionally, some of the terms in the RHS of (3.14) and (3.15) can be neglected, like the second term of (3.14), because they do not contribute to stability. The three remaining terms help to improve stability, the first one giving control of the divergence of the viscoelastic stresses, the third one on the convective term and the fourth one on the pressure gradient. Similar considerations can be applied to modify equation (3.15), now considering that $P_h^\perp(\boldsymbol{\sigma}_h) = \mathbf{0}$.

As explained earlier, the previous splitting and simplification technique results in an a priori weakly consistent method. However, when the splitting approach is used in (3.15) the method fails to converge when applied to simple numerical tests. This convergence failure is independent of the approximation properties (stability and accuracy) of the method, but clearly limit its applicability. This breakdown is produced by the fact that the full residual (the sum of all terms) is usually small whereas each separate term is large (considering absolute terms). Consequently, in numerical solutions, the split term-by-term method for the constitutive equation is not as efficient as the residual based one. It is remarkable that this phenomenon occurs also in simple stationary problems, as shown in the next example.

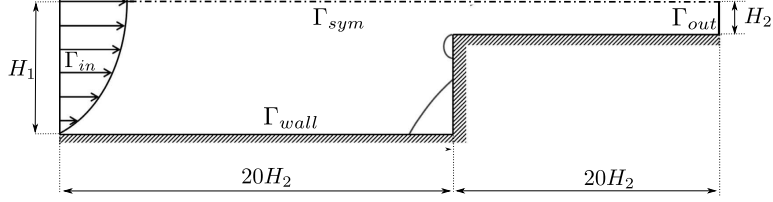


Fig. 1: Scheme of the 4:1 contraction problem.

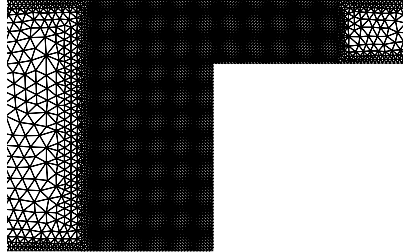


Fig. 2: Mesh used for the 4:1 contraction test.

3.2.2 Example of convergence failure of the term-by-term stabilization of the constitutive equation

In this subsection, we will briefly describe the numerical example and the results obtained when the lack of convergence for the term by term stabilization occurs. We have considered the well-known 4:1 contraction benchmark (see Figure 1) in a stationary version, with a Weissenberg number equal to 4.0 and Reynolds number equal to 0.01, as it is considered in [12], with the same boundary conditions: on the solid walls Γ_{wall} , non-slip conditions are imposed for the velocity field and on symmetric boundaries Γ_{sym} , the component y of the velocity is set to zero. Moreover, on the inlet boundary Γ_{in} a fully parabolic velocity profile and stress profile are prescribed as

$$u_x = \frac{3Q}{2H_1} \left(1 - \frac{y^2}{(2H_1)^2} \right), \quad u_y = 0,$$

$$\sigma_{xx} = 2\lambda(1-\beta)\eta_0 \left(\frac{3Q}{H_1^3} y \right)^2, \quad \sigma_{xy} = -(1-\beta)\eta_0 \left(\frac{3Q}{H_1^3} y \right), \quad \sigma_{yy} = 0,$$

where Q is the flow rate, set to 1. In this case the characteristic length is $H_1 = 4$, which is the length of the inlet channel, and $H_2 = 1$. For the outlet boundary Γ_{out} , the x component of the velocity is let free, and component y is set to zero, like the pressure. In addition, component x of the normal of the total Cauchy stress tensor is set to zero in this boundary. The space discretization consists of 7784 nodes and 14793 triangular elements, whose minimum element size is $h_{\min} = 0.05$, as it is plotted in Figure 2.

In Table 1, the different values for the terms of the constitutive equation residual are plotted for a numerical integration point situated approximately at coordinates $(17.5, -3.5)$ and for each component together with the total residual, indicated in the last row. Other points have also been checked, and the same effect is observed in all of them. The values represented in Table 1 correspond to inner-iteration 20. A continuation iterative scheme in terms of the relaxation time λ has been employed, using 15 continuation steps. Within each of them, a fixed point iterative scheme has been employed, so that $\hat{\mathbf{u}}_h$ in Table 1 is the velocity at the previous iteration of the one considered.

As it can be observed, in components xx and xy of the residual, the full residual has a smaller value than other terms such as the rotational or the convective terms separately

Residual terms	component xx	component yy	component xy
$\frac{1}{2\eta_p} \boldsymbol{\sigma}_h$	0.82002	0.68599	0.80990
$-\nabla^s \mathbf{u}_h$	0.35160	-0.41654	-0.44841
$\frac{\lambda}{2\eta_p} \hat{\mathbf{u}}_h \cdot \nabla \boldsymbol{\sigma}_h$	2.89475	-1.30149	0.74938
$-\frac{\lambda}{2\eta_p} (\boldsymbol{\sigma}_h \cdot \nabla \hat{\mathbf{u}}_h + (\nabla \hat{\mathbf{u}}_h)^T \cdot \boldsymbol{\sigma}_h)$	-4.29379	-0.59164	-2.14322
Full residual	-0.22741	-1.62369	-1.03234

Tab. 1: Values adopted by each term using the term-by-term stabilization in the constitutive equation. Inner-iteration 20.

(in absolute value). When this effect happens, the iterative scheme for the term-by-term formulation fails. Note that this occurs when the Weissemberg number is significant; if it is low, convergence does not experiment this kind of problems.

3.2.3 Final design

In view of the previous discussion, the method must be designed carefully. For this reason, along the present paper the method denoted as term-by-term (S-OSS) will be built as a split term-by-term for the momentum equation, and the full residual-based VMS, explained in Subsection 3.1, for the constitutive equation.

Under the described circumstances and following this splitting approach, we can split $\tilde{\mathbf{u}} = \tilde{\mathbf{u}}_1 + \tilde{\mathbf{u}}_2 + \tilde{\mathbf{u}}_3$, while the stress sub-grid scale remains as $\tilde{\boldsymbol{\sigma}}$. Therefore, the term-by-term finite element formulation proposed consists in finding $\mathbf{U}_h = [\mathbf{u}_h, p_h, \boldsymbol{\sigma}_h] : (0, t_f) \rightarrow \mathcal{X}_h$ such that

$$\begin{aligned} \mathcal{G}_{\text{std}}(\mathbf{U}_h, \mathbf{V}_h) + B_{\text{std}}(\mathbf{u}_h; \mathbf{U}_h, \mathbf{V}_h) + \sum_K \langle \tilde{\mathbf{u}}_1, -\rho \mathbf{u}_h \cdot \nabla \mathbf{v}_h \rangle_K \\ + \sum_K \langle \tilde{\mathbf{u}}_2, -\nabla q_h \rangle_K + \sum_K \langle \tilde{\mathbf{u}}_3, \nabla \cdot \boldsymbol{\chi}_h \rangle_K + \sum_K \langle \tilde{p}, -\nabla \cdot \mathbf{v}_h \rangle_K \\ + \sum_K \left\langle \tilde{\boldsymbol{\sigma}}, \frac{1}{2\eta_p} \boldsymbol{\chi}_h + \nabla^s \mathbf{v} - \frac{\lambda}{2\eta_p} (\mathbf{u}_h \cdot \nabla \boldsymbol{\chi}_h + \boldsymbol{\chi}_h \cdot (\nabla \mathbf{u}_h)^T + \nabla \mathbf{u}_h \cdot \boldsymbol{\chi}_h) \right\rangle_K \\ = \langle \mathbf{f}, \mathbf{v}_h \rangle, \end{aligned}$$

for all $[\mathbf{v}_h, q_h, \boldsymbol{\sigma}_h] \in \mathcal{X}_h$, where B_{std} is the bilinear form defined in (2.12), and the sub-grid scales $\tilde{\mathbf{u}}_1, \tilde{\mathbf{u}}_2, \tilde{\mathbf{u}}_3, \tilde{p}$, are the solution of the evolution problems:

$$\rho \frac{\partial \tilde{\mathbf{u}}_1}{\partial t} + \alpha_1^{-1} \tilde{\mathbf{u}}_1 = -P_h^\perp (\rho \mathbf{u}_h \cdot \nabla \mathbf{u}_h), \quad (3.16)$$

$$\rho \frac{\partial \tilde{\mathbf{u}}_2}{\partial t} + \alpha_1^{-1} \tilde{\mathbf{u}}_2 = -P_h^\perp (\nabla p_h), \quad (3.17)$$

$$\rho \frac{\partial \tilde{\mathbf{u}}_3}{\partial t} + \alpha_1^{-1} \tilde{\mathbf{u}}_3 = P_h^\perp (\nabla \cdot \boldsymbol{\sigma}_h), \quad (3.18)$$

$$\alpha_2^{-1} \tilde{p} = -P_h^\perp (\nabla \cdot \mathbf{u}_h), \quad (3.19)$$

while the sub-grid scale $\tilde{\boldsymbol{\sigma}}$ is the solution of (3.10), defined in the previous section. Parameters $\alpha_i, i = 1, 2, 3$ are the stabilization terms, already defined in (3.4)-(3.6). The proposed method is not residual-based, and therefore, is not consistent in the sense used in the finite element context, although it has an optimal consistency error.

Finally, the term-by-term stabilization proposed for the log-conformation formulation consists in finding $\mathbf{U}_h = [\mathbf{u}_h, p_h, \psi_h] : (0, t_f) \rightarrow \bar{\mathcal{X}}_h$ such that

$$\begin{aligned} \mathcal{G}_{\log}(\mathbf{U}_h, \mathbf{V}_h) + B_{\log}(\mathbf{u}_h; \mathbf{U}_h, \mathbf{V}_h) + \sum_K \langle \tilde{\mathbf{u}}_1, -\rho \mathbf{u}_h \cdot \nabla \mathbf{v}_h \rangle_K \\ + \sum_K \langle \tilde{\mathbf{u}}_2, -\nabla q_h \rangle_K + \sum_K \langle \tilde{\mathbf{u}}_3, \nabla \cdot \chi_h \rangle_K + \sum_K \langle \tilde{p}, -\nabla \cdot \mathbf{v}_h \rangle_K \\ + \sum_K \left\langle \tilde{\boldsymbol{\sigma}}, \frac{1}{2\eta_p} \chi_h + \nabla^s \mathbf{v} - \frac{\lambda}{2\eta_p} (\mathbf{u}_h \cdot \nabla \chi_h + \chi_h \cdot (\nabla \mathbf{u}_h)^T + \nabla \mathbf{u}_h \cdot \chi_h) \right\rangle_K \\ = \langle \mathbf{f}, \mathbf{v}_h \rangle, \end{aligned}$$

for all $[\mathbf{v}_h, q_h, \chi_h] \in \mathcal{X}_h$, where B_{\log} is the bilinear form defined in (2.19), the sub-grid scale $\tilde{\mathbf{u}}_3$, is now defined as the solution of:

$$\rho \frac{\partial \tilde{\mathbf{u}}_3}{\partial t} + \alpha_1^{-1} \tilde{\mathbf{u}}_3 = P_h^\perp \left(\frac{\eta_p}{\lambda_0} \nabla \cdot (\exp(\psi_h)) \right). \quad (3.20)$$

The sub-grid scales $\tilde{\mathbf{u}}_1$, $\tilde{\mathbf{u}}_2$, and \tilde{p} are solutions of (3.16), (3.17), (3.19), respectively, and the sub-grid scale $\tilde{\boldsymbol{\sigma}}$ is the solution of (3.13). Additionally, the parameters $\alpha_i, i = 1, 2, 3$ are defined in (3.4)-(3.6).

3.3 Discretization of the equations for the sub-grid scales

The time dependent behaviour of the sub-grid scales is widely analized in [2, 5], although in this Subsection we try to describe the main ideas for the two methods presented in this work: the residual-based method and the term-by-term one. For both, we have used the BDF1 scheme to discretize the defined sub-grid scales. Particularly, in the case of the split stabilization method, sub-grid scales (3.16) -(3.18) and the elastic stress sub-grid scale (3.10) can be written as

$$\begin{aligned} \tilde{\mathbf{u}}_1^{n+1} &= \left(\rho \frac{1}{\delta t} + \frac{1}{\alpha_1^{n+1}} \right)^{-1} \left(\rho \frac{1}{\delta t} \tilde{\mathbf{u}}_1^n - \rho P_h^\perp (\mathbf{u}_h^{n+1} \cdot \nabla \mathbf{u}_h^{n+1}) \right), \\ \tilde{\mathbf{u}}_2^{n+1} &= \left(\rho \frac{1}{\delta t} + \frac{1}{\alpha_1^{n+1}} \right)^{-1} \left(\rho \frac{1}{\delta t} \tilde{\mathbf{u}}_2^n - P_h^\perp (\nabla p_h^{n+1}) \right), \\ \tilde{\mathbf{u}}_3^{n+1} &= \left(\rho \frac{1}{\delta t} + \frac{1}{\alpha_1^{n+1}} \right)^{-1} \left(\rho \frac{1}{\delta t} \tilde{\mathbf{u}}_3^n + P_h^\perp (\nabla \cdot \boldsymbol{\sigma}_h^{n+1}) \right), \\ \tilde{\boldsymbol{\sigma}}^{n+1} &= \left(\frac{\lambda}{2\eta_p} \frac{1}{\delta t} + \frac{1}{\alpha_3^{n+1}} \right)^{-1} \left(\frac{\lambda}{2\eta_p} \frac{1}{\delta t} \tilde{\boldsymbol{\sigma}}^n + \tilde{P} \left(-\frac{1}{2\eta_p} \boldsymbol{\sigma}_h^{n+1} + \nabla^s \mathbf{u}_h^{n+1} \right. \right. \\ &\quad \left. \left. - \frac{\lambda}{2\eta_p} \left(\frac{\delta \boldsymbol{\sigma}_h^{n+1}}{\delta t} + \mathbf{u}_h^{n+1} \cdot \nabla \boldsymbol{\sigma}_h^{n+1} - \boldsymbol{\sigma}_h^{n+1} \cdot \nabla \mathbf{u}_h^{n+1} - (\nabla \mathbf{u}_h^{n+1})^T \cdot \boldsymbol{\sigma}_h^{n+1} \right) \right) \right). \end{aligned}$$

From these expressions, we can conclude that the sub-grid scales depend directly on $\alpha_{1\text{dyn}} = \left(\rho \frac{1}{\delta t} + \frac{1}{\alpha_1} \right)^{-1}$ and $\alpha_{3\text{dyn}} = \left(\frac{\lambda}{2\eta_p} \frac{1}{\delta t} + \frac{1}{\alpha_3} \right)^{-1}$, where $\alpha_{1\text{dyn}}$ and $\alpha_{3\text{dyn}}$ redefine the classical stabilization parameters and now depend on the time-step size. The procedure is analogous for the logarithmic formulation, now considering (3.16), (3.17) and (3.20) for $\tilde{\mathbf{u}}_1^{n+1}$, $\tilde{\mathbf{u}}_2^{n+1}$ and $\tilde{\mathbf{u}}_3^{n+1}$, respectively, and (3.13) for $\tilde{\boldsymbol{\sigma}}^{n+1}$; the same expressions for $\alpha_{1\text{dyn}}$ and $\alpha_{3\text{dyn}}$ are used.

Concerning the new definition of the stabilization parameters, an extremely relevant study about the instability that appears when the ASGS method and the *quasi-static* sub-grid scales are employed is developed by Bochev et al. in [3]. They relate this instability to

the reduction of δt if h (element size of mesh) remains fixed, i.e. for anisotropic space-time discretizations. However, the instability described disappears automatically if $\delta t \geq C\alpha_1^{n+1}$, where C is a positive constant. Therefore it seems clear that the stabilization parameter and the time step size must be related in the *quasi-static* stabilized finite element methods. This question is justified in [8], remarking that when this inequality holds, it will be unnecessary to use dynamic sub-grid scales.

Furthermore, we can observe that for the viscoelastic flow problem parameter α_3 is also modified, but no references exist about the possible effects that this change could produce. This question will be explored and discussed along the numerical examples, in the next Section.

4 Numerical results

This Section aims to show the importance of dynamic sub-grid scales to solve viscoelastic problems, and particularly the suitability of the term-by-term stabilization method described along the paper for both possible formulations, standard and logarithmic. Firstly, in Section 4.1, we display the typical flow over a cylinder problem for $Re=100$, where the different formulations proposed are compared for several Weissenberg numbers and time steps δt . Secondly, a dynamic lid-driven cavity flow problem is presented in Section 4.2 in order to discuss the efficiency and stability of the dynamics sub-grid scales in a more complex benchmark for two different cases: a stationary one with $Re=0$, and a dynamic forced regime with $Re=100$. Finally the formulation is tested in a three-dimensional lid driven cavity in the Section 4.3 as an extension of the two-dimensional dynamic version.

4.1 Flow over a cylinder

In this Subsection, the well-known flow over a cylinder problem is used to achieve several objectives: firstly, to compare the various stabilization methods proposed (dynamic and quasi-static formulations) in terms of stability when the time step is small, and when the Weissenberg number increases. Secondly, the solution obtained with the proposed formulations when using rather coarse meshes is compared with the one obtained with a fine mesh, assessing the suitability of the methods when using coarse meshes. Lastly, the behaviour of velocity sub-grid scales is studied comparing the results of the residual-based and the term-by-term formulations.

4.1.1 Setup

The computational domain is defined as a rectangle of length 16 and width 8, with a unitary cylinder centered at point (4,0), as it is plotted in Figure 3.

The boundary conditions of the problem are as follows. The inflow velocity of the problem is prescribed in Γ_{in} as $u_x = 1$ and $u_y = 0$, while Γ_{top} and Γ_{bottom} are considered fictitious walls where $u_y = 0$ and u_x is left free. For the outflow boundary Γ_{out} the velocity is left free in both components, and finally, for the wall of the cylinder Γ_{cyl} non-slip conditions are set, that is, velocity is set to zero. Note that the stress components have been let free in all boundaries.

The benchmark has been computed for different Weissenberg numbers, defined by $We = \frac{\lambda U}{L}$, where U and L are the characteristic velocity and length respectively, and the Reynolds number, defined by $Re = \frac{\rho U L}{\eta_0}$, has been set to 100. The viscoelastic fluid parameters are: $\rho = 1$, $\beta = 0.5$ and $\eta_0 = 0.01$.

The mesh used to compute this numerical example is rather coarse, due to the fact that we aim to check that our methods do not need to fulfill the $\delta t \geq Ch^2$ inequality in order to obtain stable solutions. In other words, we show that the formulation proposed

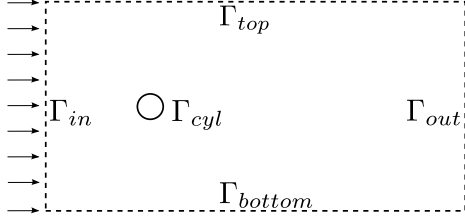


Fig. 3: Schematic representation of flow over an unconfined cylinder.

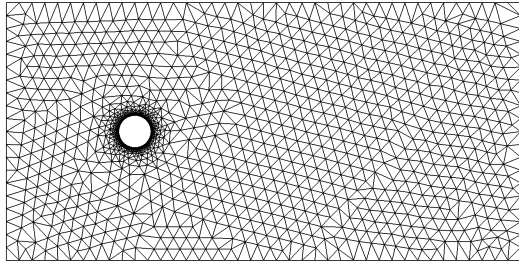


Fig. 4: Mesh employed.

is independent of the space-time discretization, without looking for an accurate result. In particular, the mesh employed is unstructured, with an element size around the cylinder of $h_{\min} = 0.01$, and coarser at the rest of the domain (maximum element size $h_{\max} = 0.4$). For the computation of this benchmark a BDF1 time discretization scheme has been used; the time step considered will be indicated in each case.

4.1.2 Stability study

First of all, we pretend to show the stability of the proposed formulation employing the time-dependent sub-grid scales explained in previous Subsections, in comparison with the quasi-static formulation. We have considered the orthogonal residual based VMS formulation (see [12]) and the term-by-term stabilization in the standard formulation. Also, a wide range of time step sizes have been contemplated to show numerically that the dynamic formulation is more stable than the quasi-static one, in particular for time steps up to $\delta t \approx \alpha_{1,\min}$ (minimum of the first stabilization parameter) for linear (P1) and quadratic (P2) elements.

Regarding the space discretization, Figure 4 has been employed to elaborate this comparative, resulting in $\alpha_{1,\min} \approx 1.156 \times 10^{-3}$ when P1 elements are considered. For P2 elements the minimum stabilization parameter is $\alpha_{1,\min} \approx 7.4 \times 10^{-5}$. Note that $\alpha_{1,\min}$ is a value obtained from each problem, and depends directly on the h (element size) magnitude .

In all these cases, the Weissenberg number has been fixed to 0.125, that is a low value, in order to avoid failures associated with a high elasticity.

Results are summarized in Table 2, where the suffix *Static* indicates the cases solved through a quasi-static method, whereas *Dyn* refers to the dynamic sub-grid scale methods. On the other hand, the term-by-term stabilization method is denoted by *SOSS* and *OSS* is labelled for the residual-based orthogonal VMS method. In both cases, linear and quadratic elements, the dynamic method is the most efficient, as it has been argued in the preceding section. In both cases (P1 and P2 elements), the most unstable stabilization method is the quasi-static formulation together with the residual-based stabilization, which is not able to solve the problem for $\delta t \lesssim 21\alpha_{1,\min}$ for linear elements. The quasi-

P1 elements		Time step (δt)		
Method		0.050	0.0250	3.125×10^{-3}
Static-OSS	Solved	Failed	-	-
Dyn-OSS	Solved	Solved	Solved	Solved
Static-SOSS	Solved	Solved	Solved	Failed
Dyn-SOSS	Solved	Solved	Solved	Solved

Tab. 2: Solved and failed cases $We = 0.125$, $\alpha_{1,\min} \approx 1.156 \times 10^{-3}$.

P2 elements		Time step (δt)		
Method		0.025	0.0125	3.906×10^{-4}
Static-OSS	Solved	Failed	-	-
Dyn-OSS	Solved	Solved	Solved	Solved
Static-SOSS	Solved	Solved	Solved	Failed
Dyn-SOSS	Solved	Solved	Solved	Solved

Tab. 3: Solved and failed cases $We = 0.125$, $\alpha_{1,\min} \approx 7.4 \times 10^{-5}$.

static formulation using a split stabilization is particularly stable in comparison with the residual based. In this case, for both types of elements, the scheme presents instabilities approximately when $\delta t \approx \alpha_{1,\min}$. For smaller time steps, only the dynamic stabilization methods achieve convergence of the problem. Note that that the instability in principle appears when the inequality $\delta t \geq C\alpha_1^{n+1}$ is not fulfilled.

A second comparative study has been carried out. In this case, the high Weissemberg number instability has been tested, solving the flow past a cylinder problem for several Weissemberg numbers. Let us recall that this dimensionless number represents the elasticity in the flow, therefore when elasticity is high the computation of the flow leads to several difficulties, among them, the exponential growth of the elastic stresses. In Table 4, the dynamic formulation of the residual-based and the term-by-term stabilization for the standard formulation and the logarithmic formulation are tested for different Weissemberg numbers. In all cases, the time step is fixed at $\delta t = 0.1$, and continuation techniques have not been employed.

Residual-based methods are the less stable ones and they fail for Weissemberg numbers equal to 0.25 and 0.375, for standard and logarithmic formulations, respectively. It is remarkable that the split term-by-term stabilization methods show a suitable robustness in spite of using the standard formulation, as it can be observed in Table 4 for $We = 0.375$. Nevertheless, the logarithmic formulation together with the dynamic sub-grid scales is the most effective method: while the other methods are not able to converge for $We = 0.5$, the dynamic logarithmic formulation is capable of converging in this case.

The conclusion is that for problems with a δt sufficiently small such that the inequality

Formulation	Weissemberg (We)			
	0.125	0.25	0.375	0.5
Std-OSS	Solved	Failed	-	-
Std-SOSS	Solved	Solved	Solved	Failed
Log-OSS	Solved	Solved	Failed	-
Log-SOSS	Solved	Solved	Solved	Solved

Tab. 4: Solved and failed cases for the two dynamic formulations (Std: Standard and Log: Logarithmic), $\delta t = 0.1$.

	Weissemberg (We)			
Formulation	0.125	0.165	0.25	0.5
Std-Static	Solved	Failed	-	-
Std-Dyn	Solved	Solved	Solved	Failed
Log-Static	Solved	Solved	Failed	-
Log-Dyn	Solved	Solved	Solved	Solved

Tab. 5: Solved and failed cases for S-OSS formulations, dynamic and quasi-static, $\delta t = 0.1$.

$\delta t \geq C\alpha_1^{n+1}$ is not satisfied (at a certain time step n), and whose Weissemberg number is particularly high, only a dynamic term-by-term logarithmic formulation will be effective. We have tested numerically that if, for instance, $\delta t = 1.562 \times 10^{-3}$ for P1 elements is used, only the dynamic term-by-term stabilization is stable (see Table 2). However, if we contemplate a flow with a Weissemberg number equal to 0.5, this model would not be able to converge unless a logarithmic formulation is used.

Finally, a study has been performed, putting the focus on the Split-OSS methods and how the dynamic formulation can affect stability not only when the time step is small, but also in terms of elasticity. In Table 5 the most significant results have been summarized, the conclusion being that dynamic formulations are more efficient avoiding elastic instabilities, permitting the computation of fluid flows with a higher Weissemberg number. For example, for the logarithmic conformation formulation, $\alpha_{1,\min} \approx \alpha_{1\text{dyn},\min} \approx 0.119 \times 10^{-2}$, i.e., the stabilization parameter of the momentum equation remains similar in both problems, dynamic and quasi-static, while the constitutive stabilization parameter differs significantly ($\alpha_{3,\min} \approx 0.335 \times 10^{-2}$ and $\alpha_{3\text{dyn},\min} \approx 0.562 \times 10^{-4}$). This is due to the structure of the dynamic parameter, which apart from depending on time step size also depends on the parameter λ , directly related with the dimensionless Weissemberg number.

It is clear that the logarithmic formulation is more expensive than the standard one due to the computations of the exponential of the variable ψ , among others [11]; this needs to be taken into account when selecting the proper formulation and stabilization method for a given problem. In Figure 5 a general scheme has been displayed for the Split-OSS formulations, where the characteristics of the problem determine the use of dynamic/quasi-static sub-grid scales and logarithmic/standard formulations. The vertical axis represents the Weissemberg number magnitude, and the horizontal axis corresponds the size of the time step. In this case, labels “big” and “small” refer to magnitudes in comparison with the stabilization parameter $\alpha_{1,\min}$ and the quoted inequality $\delta t \geq C\alpha_1^{n+1}$ for all n . Note that the thresholds are not sharp, due to the fact that the dynamic stabilization is also useful to deal with some high Weissemberg problems and it could avoid the need of using the logarithmic formulation to solve them, which is much more expensive from the computational point of view.

4.1.3 Comparison between methods

In this subsection we compare the solution obtained by using the proposed methods considering a low Weissemberg value, set to 0.125.

Firstly, in Figure 6, pressure, velocity and stress have been plotted for the solution obtained with the dynamic term-by-term formulation, considering a time step $\delta t = 0.1$, for linear (left) and quadratic (right) elements. The differences found between the results obtained with P1 and P2 elements are due to the coarse discretization used; due to this, solutions obtained using P2 elements are more accurate and less mesh-dependent. Note that for higher Weissemberg numbers, the results are very similar qualitatively, with the

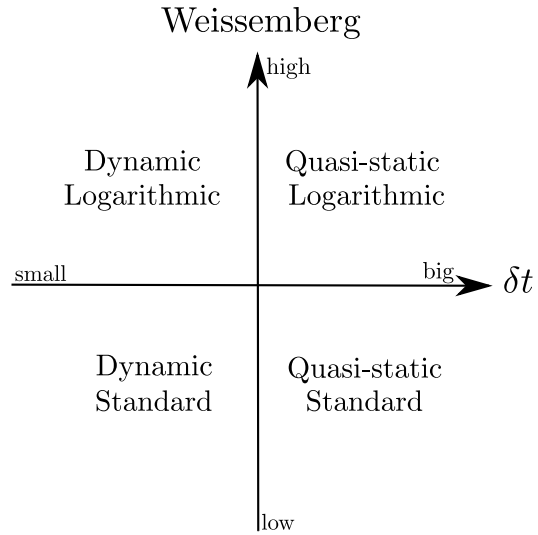


Fig. 5: A general scheme of S-OSS formulations and methods.

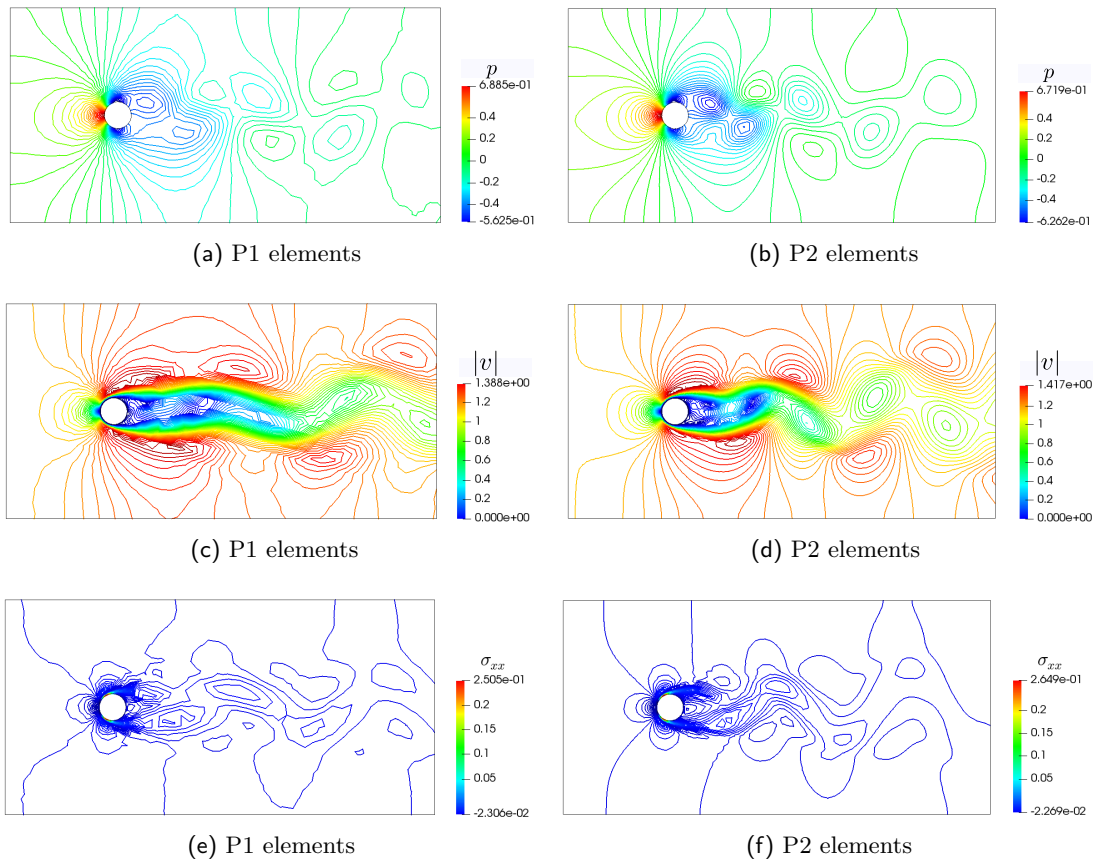


Fig. 6: Isolines of the pressure, velocity and component xx of the elastic stress, $\delta t = 0.1$.

exception of the elastic stress tensor, whose maximum values increase significantly on the wall of the cylinder.

The evolution of the main fields in a downstream point situated at $(6, 0)$ is displayed in order to compare the solution between stabilization methods in Figure 7. The graphs show curves along time when oscillatory solutions are achieved for the second component of the velocity, the pressure and the xx component of the stresses. Also, results are depicted for different time step sizes: for $\delta t = 0.1$ and for $\delta t = 1.5625 \times 10^{-3}$, in other words, $\delta t \approx \alpha_{1,\min}$. For the smaller time step, only the dynamic methods are stable, as detailed in Table 2, for this reason only OSS and S-OSS dynamic cases are taken into account.

As explained in [8], the instability derived from the space-time discretization restriction can be identified in the evolution of pressure, as shown in Figure 7c when the static OSS stabilization method is used.

On the other hand, in Figure 7a we can observe that the quasi-static sub-grid scales together with the residual-based stabilization is the less dissipative one, followed by the dynamic sub-grid scales version. In comparison, the term-by-term formulation is more diffusive than the orthogonal residual-based methods. Additionally, the dynamic formulation is also more dissipative than the quasi-static version.

We need to remark that the differences between the residual-based and the term-by-term formulations appreciated in Figure 7 are caused directly by the coarse mesh employed, since for finer discretizations no significant differences are found.

The next figures show an interesting result. In Figures 8 and 9 the components x and y of the sub-grid scales are plotted for both dynamic formulations utilized: the orthogonal residual, denoted by $\tilde{\mathbf{u}}$, and the split term-by-term, denoted in Figures 8 and 9 as $\tilde{\mathbf{u}}_1$, $\tilde{\mathbf{u}}_2$ and $\tilde{\mathbf{u}}_3$. At first sight, the sub-grid scales obtained by the split formulation are very different to the ones of the orthogonal residual method. The existence of a difference between both methods is evident, because while in the term-by-term formulation only local inner products of the convective term, the pressure gradient and the divergence of the stress are considered, the residual stabilization takes into account all of the cross product terms of these operators applied to the unknowns and the test functions. Furthermore, the sub-grid scales of the velocity are not similar in both methods. However, when the three sub-grid scales are added (denoted by $\sum_{i=1}^3 \tilde{\mathbf{u}}_i$), the result is very similar to the sub-grid scales obtained with the residual based formulation, as illustrated in Figures 8 and 9. This effect has already been reported for the Navier-Stokes problem in [8]. The results for quadratic elements are shown in Figure 9. The general trend is similar too, although the presence of the Laplacian term in the residual-based formulation is probably the cause for the observed differences.

In this case, the solutions obtained with the logarithmic formulations are identical to the standard formulation. For this reason, the type of formulation (standard or logarithmic reformulation) has not been specified in this comparative.

4.2 Lid-driven cavity flow problem

The lid-driven cavity flow is a good example to illustrate the differences that can be generated by the viscoelastic contribution in the fluid, due to the elastic stresses dependance on the previous deformation history. In this case, we have solved it to prove that the dynamic term-by-term formulation is also efficient.

4.2.1 Steady-state case at $\text{Re} = 0$

A fluid confined in the unit square is considered, whose boundaries are solid walls except the top boundary, which has a prescribed velocity in the x direction, as shown in Figure 10a. Because the viscoelastic fluid cannot sustain deformation at a stagnation point, the

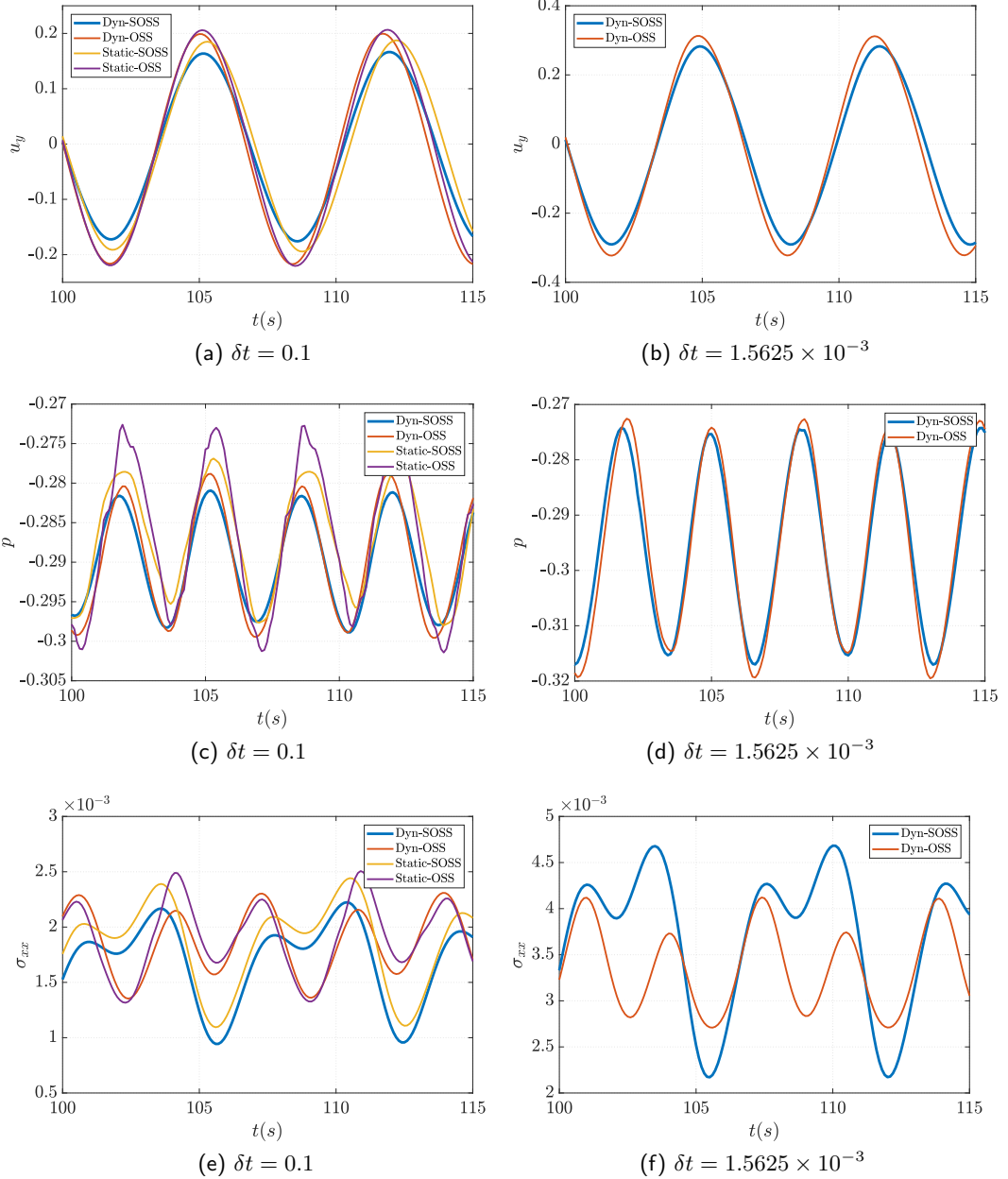


Fig. 7: Comparison between the different stabilization methods and $\delta t = 0.1$ (left) and $\delta t = 0.0015625$ (right).

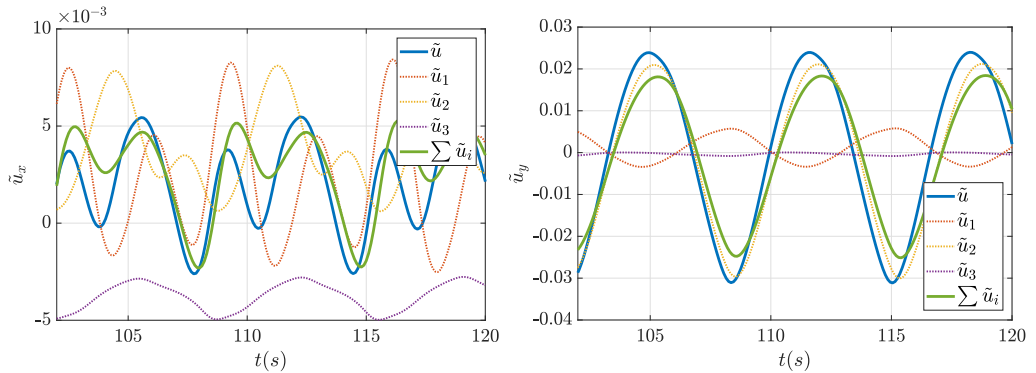


Fig. 8: Comparison of the sub-grid scales at $\delta t = 0.1$, P1 elements.

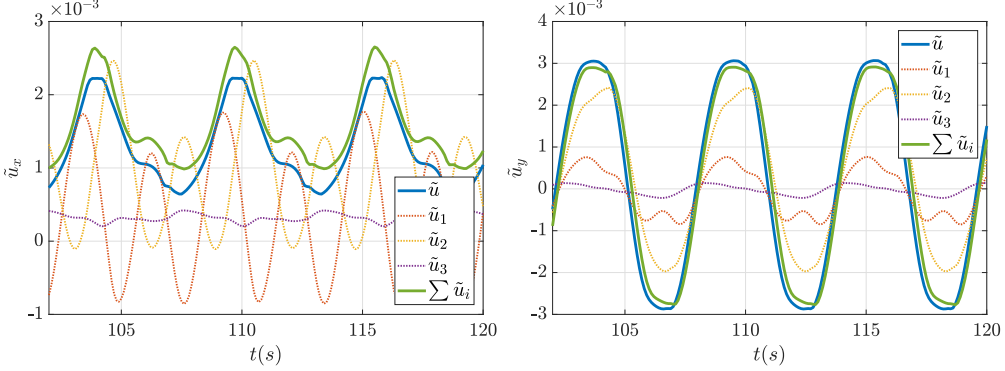


Fig. 9: Comparison of the sub-grid scales at $\delta t = 0.1$, P2 elements.

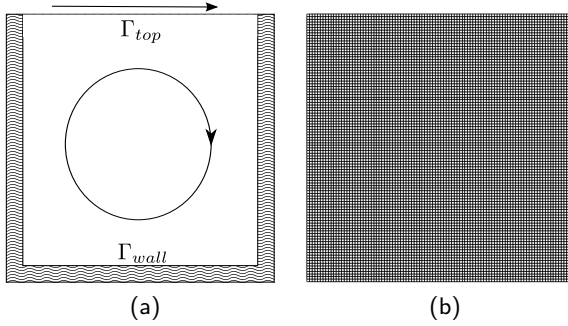


Fig. 10: Schematic representation of lid driven cavity (a) and Mesh used (b).

motion of the lid must be smooth and the gradient of the velocity should be zero at corners. For this reason, on the boundary Γ_{top} the horizontal velocity has been chosen as follows:

$$u_x(x, 1, t) = 8 \left[1 + \tanh \left(8 \left(t - \frac{1}{2} \right) \right) \right] x^2 (1-x)^2,$$

$$u_y(x, 1, t) = 0,$$

where the function $1 + \tanh(8(t - \frac{1}{2}))$ has a smooth transition, being zero at $t = 0$; u_x attains the maximum value ($u = 1$) when $t > \frac{1}{2}$ at the center, $x = \frac{1}{2}$. In Γ_{wall} , velocity is set to zero in both components. The inflow boundary conditions for the elastic stress tensor are not needed since there is no inflow boundary in this problem. As characteristic velocity, the maximum lid velocity has been taken to compute the dimensionless numbers, and the characteristic length is 1, the size of each square's side. The considered Weissenberg number is $We = 1.0$, and the Reynolds number $Re = 0$. Referring to the spatial discretization, a structured mesh composed by 10000 bilinear Q1 elements is used (see Figure 10b) and the time step considered is $\delta t = 0.0025$. Referring to the time discretization scheme, a BDF1 scheme has been used.

This test is carried out with the aim of comparing the accuracy of the dynamic and the quasi-static stabilization methods in a stationary problem, comparing the results with other authors [9, 20, 21, 22]. In our case neither continuation iterative methods to treat the convergence, nor additional sub-relaxation schemes have been employed.

In Table 6 we show that the problem is solved successfully only for the combination of the logarithmic formulation and the dynamic sub-grid scale stabilization. The steady state tolerance is 10^{-5} , and for each time step three non-linear Newton-Raphson iterations are employed. As in the cylinder example, $\alpha_{1,\min} \approx 0.83 \times 10^{-5} \approx \alpha_{1\text{dyn},\min}$, therefore the dynamic sub-grid scales for the momentum equations are not peremptory because the instability is not originated by a small time step. In this case, the high Weissenberg

Stabilization S-OSS		
Formulation	Quasi-static	Dynamic
Standard	Failed - time step 265	Failed - time step 1316
Logarithmic	Failed - time step 240	Solved

Tab. 6: Comparison between different formulations, $We = 1.0$, $\delta t = 0.0025$. The time step at which convergence fails is indicated.

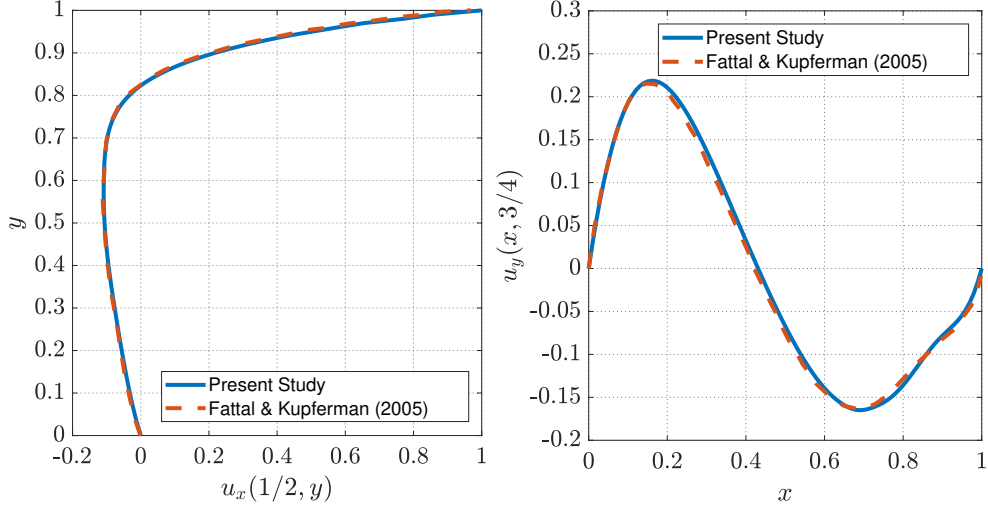


Fig. 11: Results at time $t = 8$, for $We = 1$. Velocity profiles along the lines $x = 1/2$ and $y = 3/4$.

number is the main problem. If we compare the stabilization methods, we see that $\alpha_{3,\min} \approx 0.25$, whereas $\alpha_{3\text{dyn},\min} \approx 0.239 \times 10^{-2}$. This notable difference is due to the structure of parameter $\alpha_{3\text{dyn},\min}$, which depends directly on the magnitude of λ . This structure of the parameter combined with the log-conformation formulation allows to properly solve this problem. It can be observed that while the quasi-static options fail early in the simulation, even in the log-conformation reformulation, the dynamic stabilization is, from this point of view, much more efficient for high Weissemberg numbers.

It must be remarked that although in [21], convergence was achieved with a quasi-static and standard formulation, a fractional step scheme was used to solve it, together with some continuation and sub-relaxation methods to help convergence, while in our case only a monolithic method with a fixed point iterative scheme without extra sub-relaxation artifacts is considered.

In Figure 11, cuts of the velocity components have been displayed, whereas in Figure 12 cuts of the components of ψ are plotted with the aim of comparing the results with other works such as [9, 23, 22]. The results are extremely similar to those by Fattal and Kupferman. For the component ψ_{yy} , the solution is compared with the results in [22]. The small differences found between our work and other publications probably are due to the differences with the mesh used. For example, in [22] the mesh employed is extremely fine near the boundaries in contrast with the uniform relatively coarse mesh used in our case.

4.2.2 Dynamic case at $Re = 100$

In this case the boundary conditions are similar to the steady-state case, with the exception of the condition imposed over the boundary Γ_{top} , where now the horizontal velocity has

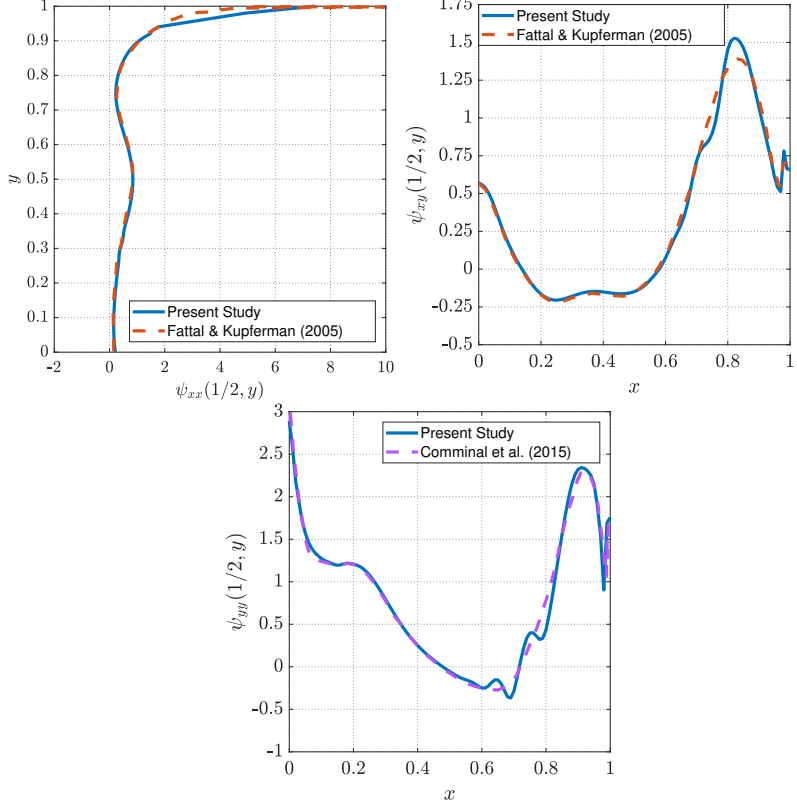


Fig. 12: Results at time $t = 8$, for $\text{We} = 1$. ψ profiles along the lines $x = 1/2$ and $y = 3/4$.

been selected as:

$$\begin{aligned} u_x(x, 1, t) &= 16x^2(1-x)^2 \sin(\pi t), \\ u_y(x, 1, t) &= 0. \end{aligned}$$

The $\sin(\pi t)$ term has been added to force the lid velocity to be time dependent and dynamic. Additionally, the Reynolds number ($\text{Re} = \frac{\rho UL}{\eta_0}$) will be considered equal to 100.

The mesh and time-step size considered are the ones defined in the stationary case, but in this occasion the time discretization scheme is BDF2. We will show the results obtained under the assumptions commented, and these will be compared with the solution shown in [21], where the authors studied the same benchmark in the quasi-static case employing a fractional step method developed in the same work.

If the time step is small, the quasi-static method is incapable of solving the dynamic problem, considering that now the stabilization parameter is $\alpha_{1,\min} \approx 4.1 \times 10^{-4}$. In Figure 13, streamlines are displayed for two different time steps, $t = 1.5$ and $t = 2.0$, and in Figure 14 the component σ_{xy} of the stress has been plotted. These results are shown in order to do a qualitative study, similar snapshots are presented in [8]. In addition, in Figure 14 the isolines that correspond to the component xy of the stress sub-grid scale have been presented as isocontours. The same case has been checked for the dynamic logarithmic formulation, obtaining similar results.

4.3 Three-dimensional case

In order to check that the proposed stabilization method works well also in the three-dimensional case, we have simulated the lid driven cavity problem in the 3D case. The problem is just an extension of the two-dimensional case developed in Subsection 4.2.

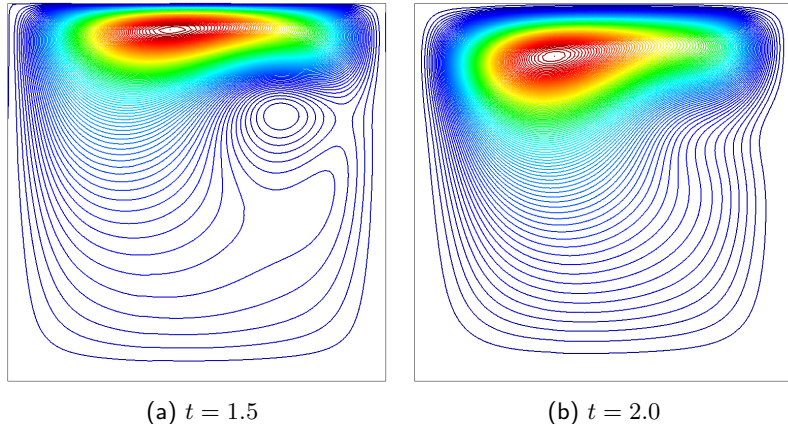


Fig. 13: Streamlines in the lid-driven cavity, using the dynamic Split OSS method.

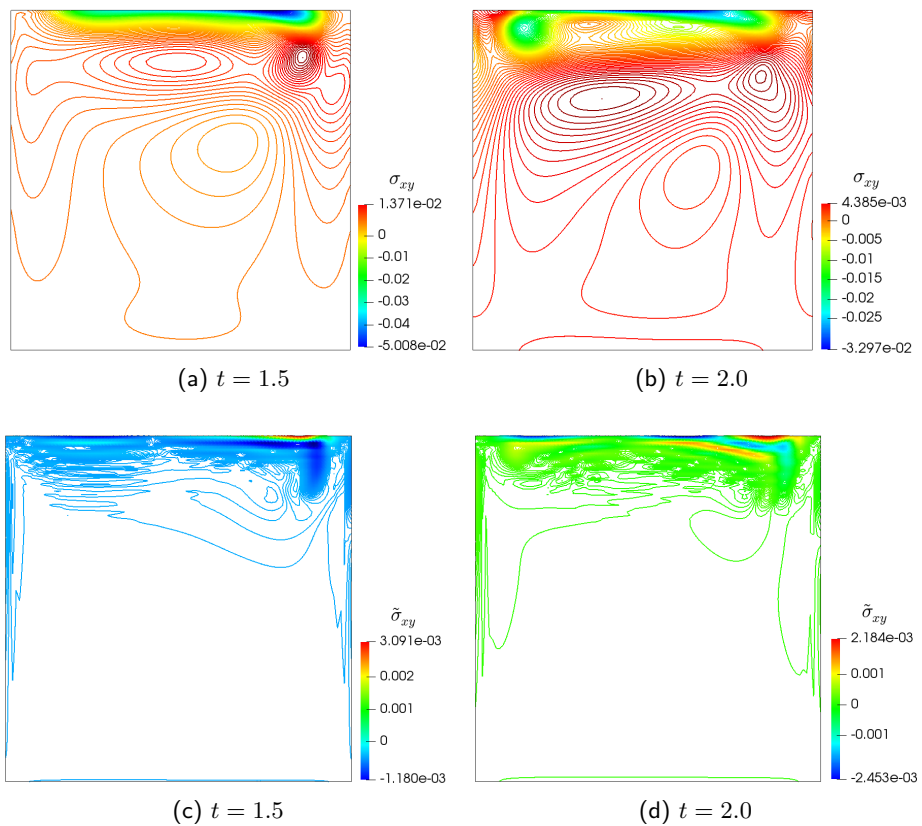


Fig. 14: Isolines of the component xy of the stresses (top), and of the sub-grid scale (bottom), using the Split OSS method.

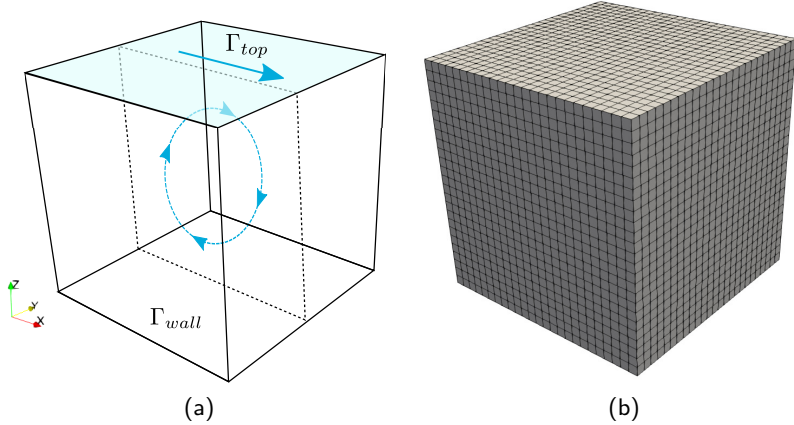


Fig. 15: Schematic representation of lid driven cavity 3D (a) and mesh used (b).

4.3.1 Setup

The three-dimensional lid driven cavity problem is solved for an unit cube, as displayed in Figure 15a. On the top of the lid (denoted by Γ_{top} in the scheme) the components of the velocity are prescribed to:

$$\begin{aligned} u_x(x, y, 1, t) &= 256x^2(1-x)^2y^2(1-y)^2 \sin(\pi t), \\ u_y(x, y, 1, t) &= 0, \\ u_z(x, y, 1, t) &= 0, \end{aligned}$$

and velocity is fixed to zero at the rest of boundaries (Γ_{wall}). Similar to Subsection 4.2, the boundary condition imposed on the top is due to two reasons: on the one hand the necessity of imposing a smooth condition at the corners, and on the other hand the necessity of a time-dependent boundary to make the problem dynamic. As in the two-dimensional case, no boundary conditions are required for the stresses. The physical properties considered for the problem are a Weissenberg number of 0.5 and a Reynolds number equal to 100.

The numerical spatial discretization consists in 15625 trilinear Q1 hexaedral elements, and 17576 nodes, plotted in Figure 15b. Finally, referring to the time discretization, a BDF1 time integrator is employed together with a time step size of $\delta t = 0.01$ and a time interval from 0 to 2 seconds.

4.3.2 Results

The aim of this problem is to demonstrate that the dynamic sub-grid scale formulation is able to solve three-dimensional cases; we do not have any reference to compare the accuracy of our results, although the mesh employed can be considered coarse for the problem being solved. No significant differences have been found between our results and those reported in [21].

In Figure 16 we have plotted isolines of some relevant fields in cuts defined by planes $x = 0.5$, $y = 0.5$ and $z = 0.5$, at time $t = 1.5$. In particular, Figure 16a shows the distribution of the pressure, Figure 16b the first component of the velocity, and finally, Figures 16c and 16d display the distribution of the component xy of the stresses and the sub-grid scales of the stresses, respectively. The problem has been run using the dynamic term-by-term standard and logarithmic formulations, obtaining very similar results.

Streamlines in the cut-plane $y = 0.5$ and for two different times ($t = 1.5$ and $t = 2.0$) are shown in Figure 17.

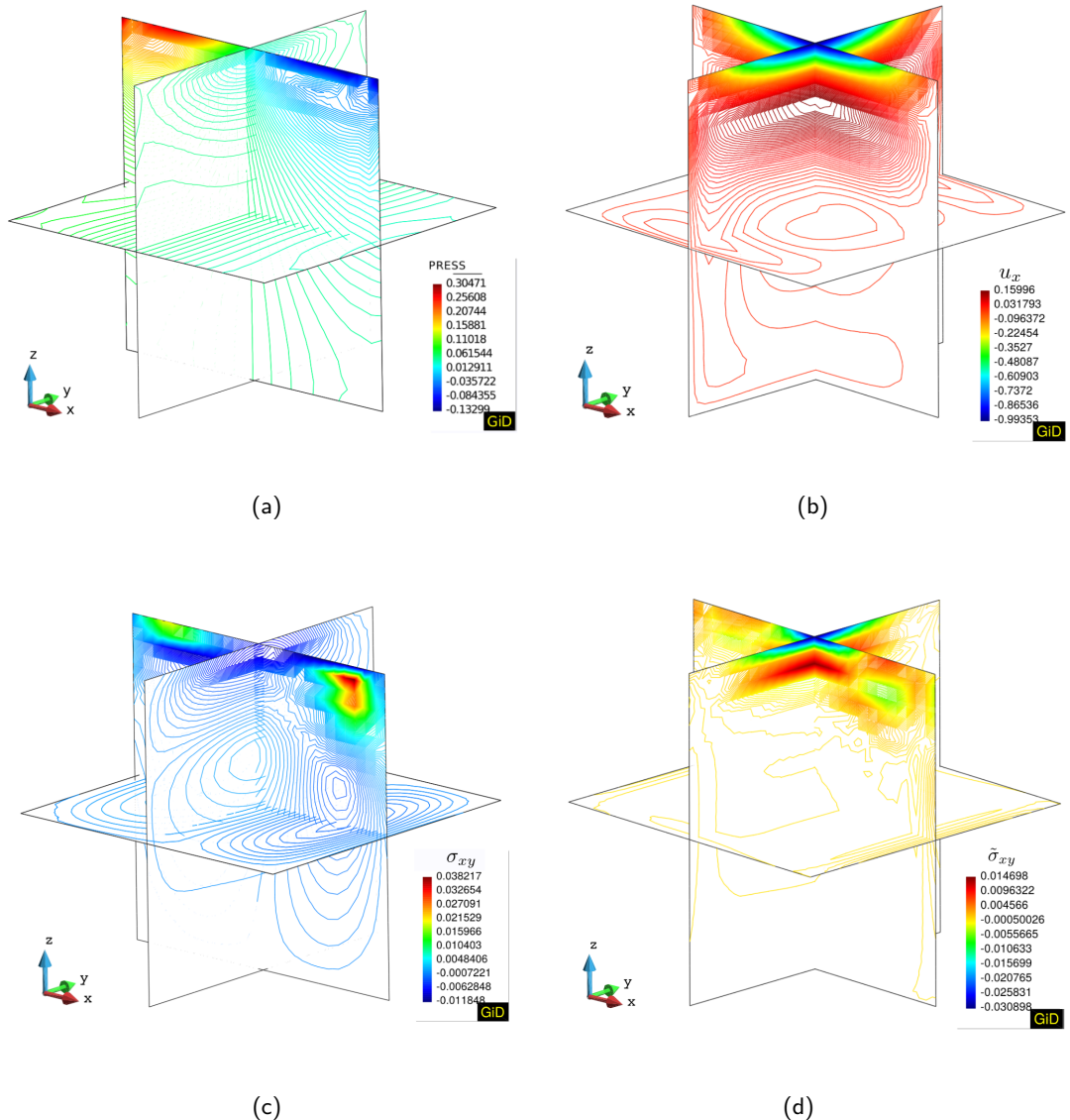


Fig. 16: Isolines in some cuts in Lid-driven cavity 3D, in $t = 1.5$.

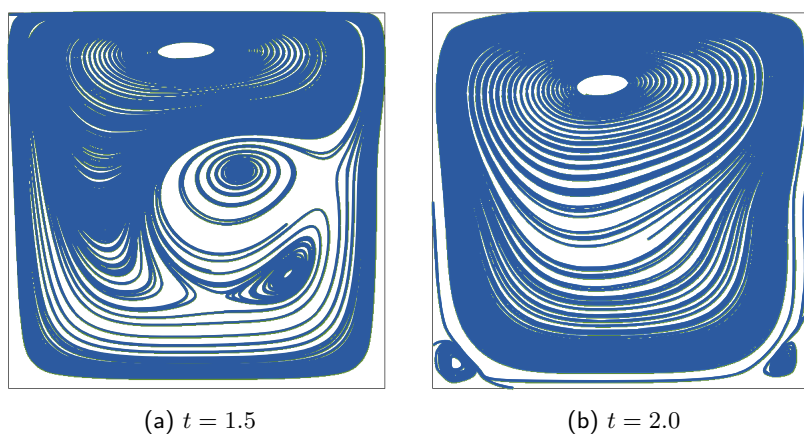


Fig. 17: Streamlines in a cut-plane $y = 0.5$

5 Conclusions

Along this work, various dynamic sub-grid scales VMS-stabilization methods have been proposed with the goal of solving viscoelastic flow problems. The main ideas have been applied to the log-conformation reformulation [10] of the viscoelastic equations, originally proposed in [11]. For both formulations (standard and logarithmic), two different stabilization methods have been designed: one based on the residual of the equations, and the second one based on a split term-by-term stabilization for the momentum equation. The stabilized methods defined in this work allow to solve time-dependent problems typically where two different sources of instability can appear simultaneously: the one originated by anisotropic space-time refinement when the time step is small and the well-known stress exponential growth typical of high Weissemberg numbers of viscoelastic problems.

The proposed methods have been analyzed extensively in several benchmarks, using linear and quadratic elements, structured and unstructured meshes, doing different comparatives between the quasi-static and dynamic stabilization methods to show the efficiency and robustness of the new strategies. The results obtained are particularly remarkable due to the high Weissemberg number reached with the dynamic formulation, which remains stable even if the standard formulation is considered, apart from evident benefits in anisotropic space-time discretizations when the time step is small. The combination of dynamic sub-grid scales and the logarithmic formulation is capable of solving problems with higher elasticity, although this formulation is more expensive. Finally, the formulation also shows good results for the three-dimensional case.

Acknowledgements

Laura Moreno acknowledges the support received from the Spanish Government through a predoctoral FPI Grant. Ramon Codina acknowledges the support received from the ICREA Acadèmia Research Program of the Catalan Government. Joan Baiges acknowledges the support of the Spanish Government through the Ramón y Cajal grant RYC-2015-17367. This work is partially funded through the ELASTIC-FLOW project, Ref. DPI2015-67857-R of the Spanish Government.

References

- [1] P. B. Bochev, M. D. Gunzburger, and J. N. Shadid. On inf-sup stabilized finite element methods for transient problems. *Computer Methods in Applied Mechanics and Engineering*, 193(15-16):1471–1489, 2004.
- [2] S. Badia and R. Codina. On a multiscale approach to the transient Stokes problem. *Transient subscales and anisotropic space-time discretization*. Preprint, 2007.
- [3] P. B. Bochev, M. D. Gunzburger, and R. B. Lehoucq. On stabilized finite element methods for the Stokes problem in the small time step limit. *International Journal for Numerical Methods in Fluids*, 53(4):573–597, 2007.
- [4] T.J.R. Hughes, G. R. Feijóo, L. Mazzei, and J. Quincy. The variational multiscale method. A paradigm for computational mechanics. *Computer methods in applied mechanics and engineering*, 166(1-2):3–24, 1998.
- [5] R. Codina, J. Principe, O. Guasch, and S. Badia. Time dependent subscales in the stabilized finite element approximation of incompressible flow problems. *Computer Methods in Applied Mechanics and Engineering*, 196(21-24):2413–2430, 2007.

- [6] R. Codina. Stabilized finite element approximation of transient incompressible flows using orthogonal subscales. *Computer Methods in Applied Mechanics and Engineering*, 191(39-40):4295–4321, 2002.
- [7] O. Colomés, S. Badia, R. Codina, and J. Príncipe. Assessment of variational multi-scale models for the large eddy simulation of turbulent incompressible flows. *Computer Methods in Applied Mechanics and Engineering*, 285:32–63, 2015.
- [8] E. Castillo and R. Codina. Dynamic term-by-term stabilized finite element formulation using orthogonal subgrid-scales for the incompressible Navier-Stokes problem. *Computer Methods in Applied Mechanics and Engineering*, 349:701–721, 2019.
- [9] R. Fattal and R. Kupferman. Time-dependent simulation of viscoelastic flows at high Weissenberg number using the log-conformation representation. *Journal of Non-Newtonian Fluid Mechanics*, 126(1):23–37, 2005.
- [10] R. Fattal and R. Kupferman. Constitutive laws for the matrix-logarithm of the conformation tensor. *Journal of Non-Newtonian Fluid Mechanics*, 123(2-3):281–285, 2004.
- [11] L. Moreno, R. Codina, J. Baiges, and E. Castillo. Logarithmic conformation reformulation in viscoelastic flow problems approximated by a VMS-type stabilized finite element formulation. *Submitted*.
- [12] E. Castillo and R. Codina. Variational multi-scale stabilized formulations for the stationary three-field incompressible viscoelastic flow problem. *Computer Methods in Applied Mechanics and Engineering*, 279:579–605, 2014.
- [13] E. Castillo and R. Codina. Stabilized stress–velocity–pressure finite element formulations of the Navier–Stokes problem for fluids with non-linear viscosity. *Computer methods in applied mechanics and engineering*, 279:554–578, 2014.
- [14] R. Codina, S. Badia, J. Baiges, and J. Príncipe. Variational Multiscale Methods in Computational Fluid Dynamics. *Encyclopedia of Computational Mechanics, Second Edition*, pages 1–28, 2018.
- [15] R. Codina. A stabilized finite element method for generalized stationary incompressible flows. *Computer Methods in Applied Mechanics and Engineering*, 190(20-21):2681–2706, 2001.
- [16] S. Badia, R. Codina, and J. V. Gutiérrez-Santacreu. Long-term stability estimates and existence of a global attractor in a finite element approximation of the Navier–Stokes equations with numerical subgrid scale modeling. *SIAM Journal on Numerical Analysis*, 48(3):1013–1037, 2010.
- [17] T. C. Rebollo. A term by term stabilization algorithm for finite element solution of incompressible flow problems. *Numerische Mathematik*, 79(2):283–319, 1998.
- [18] R. Codina. Stabilization of incompressibility and convection through orthogonal sub-scales in finite element methods. *Computer methods in applied mechanics and engineering*, 190(13-14):1579–1599, 2000.
- [19] R. Codina. Analysis of a stabilized finite element approximation of the oseen equations using orthogonal subscales. *Applied Numerical Mathematics*, 58(3):264–283, 2008.

- [20] P. Saramito. On a modified non-singular log-conformation formulation for Johnson–Segalman viscoelastic fluids. *Journal of Non-Newtonian Fluid Mechanics*, 211:16–30, 2014.
- [21] E. Castillo and R. Codina. First, second and third order fractional step methods for the three-field viscoelastic flow problem. *Journal of Computational Physics*, 296:113–137, 2015.
- [22] R. Comminal, J. Spangenberg, and J. H. Hattel. Robust simulations of viscoelastic flows at high Weissenberg numbers with the streamfunction/log-conformation formulation. *Journal of Non-Newtonian Fluid Mechanics*, 223:37–61, 2015.
- [23] J. Hao and T.W. Pan. Simulation for high Weissenberg number: viscoelastic flow by a finite element method. *Applied mathematics letters*, 20(9):988–993, 2007.